DEVELOPING METHODS TO DIFFERENTIATE SPECIES AND ESTIMATE COVERAGE OF BENTHIC AUTOTROPHS IN THE POTOMAC USING DIGITAL IMAGING

By

Kevin Stanfield

B.A. (University of Kentucky) 2009

THESIS

Submitted in Partial satisfaction of the requirements

For the degree of

MASTER OF SCIENCE

in

ENVIRONMENTAL BIOLOGY

in the

GRADUATE SCHOOL

Of

HOOD COLLEGE

May 2018

Accepted:

_____
Kevin Sellner, Ph.D.
Committee Member

_____
George Dimitoglou, Ph.D
Committee Member

_____
Susan Carney, Ph.D.
Program Director, Environmental Biology

_____
Drew Ferrier, Ph.D.
Thesis Adviser

_____
April Boulton, Ph.D.
Dean of the Graduate School

STATEMENT OF USE AND COPYRIGHT WAIVER

I authorize Hood College to lend this thesis, or reproductions of it, in total or in part, at the request of other institutions or individuals for the purpose of scholarly research.

ABSTRACT

This study developed methods for the quantification of benthic autotroph coverage in the Upper Potomac using digital imagery captured with drone-mounted cameras. Submerged aquatic vegetation (SAV) is an integral part of freshwater ecosystems and the presence or absence and abundance of SAV can be used as a barometer for ecosystem health. Cyanobacteria blooms occur regularly in the Upper Potomac during summer months and may be releasing cyanotoxins into the water. Drone imagery offers an easy and inexpensive way of generating coverage estimate of SAV and cyanobacteria which can then be used to assess ecological conditions. This study was able to differentiate substrate and benthic autotrophs with imagery captured at low altitude with 3 and 5-band cameras. This study also offers suggestions for differentiating between SAV and cyanobacteria if equipment with finer spectral resolution is available.

ACKNOWLEDGMENTS AND SPONSORSHIP

My experience at Hood College has been entirely positive, and I am very grateful for the opportunities provided by the college. This thesis would not have been possible without a grant from the Hood College Graduate Research Fund.

I would like to thank the many people from Hood College who came together to help me complete this thesis. Kevin Sellner, George Dimitoglou, and Drew Ferrier put a lot of effort into improving my scientific design and writing, and were willing to work with my accelerated schedule to ensure that I graduated on time. I learned a lot from them and truly enjoyed working with them. Peter O'Connor and Abbi Strock piloted drones and kayaks for me, respectively. They were willing to begin working very early in the morning and continue until the work was done. Eric Kindahl and Randy Smith fielded many strange GIS questions and helped me think through several problems. I would also like to thank Sue Carney, Eric Annis, Ricky Hirschhorn, Oney Smith, Kathy Falkenstein, Georgie Jones, Miranda Darby, Craig Laufer, Jen Krishnaswamy, Hans Wagner, Bianca Hoch, and Nathan Reetz for equal measures of heartwarming encouragement and relentless harassment, providing the perfect environment for productivity.

I also received a lot of help from outside Hood College. Michael Kashiwagi and Josh Henesy from MD DNR provided input on the research design and baseline data for my study. Billie Griffith and Yakov Pachepsky from USDA provided input on the research design, and loaned out a drone with a multispectral camera which Billie piloted for my project. Shelly Tomlinson from NOAA provided input on research design and provided spectral signatures which she had collected for some of the targets of this study.

Finally, I would like to thank several family members and personal friends who helped me with this project. Dana Doggett, Ed Stanfield, and John Buxbaum were kind enough to listen to me talk about my research on a weekly basis for two years. Cindy Doggett, in addition to constant encouragement, loaned me two kayaks for use in this study. Maureen Meyers, Scott Hutson, and Kevin Clark all played a part in teaching me the importance of both academic integrity and having fun while you work hard.

TABLE OF CONTENTS

LIST OF TABLES

LIST OF FIGURES

LIST OF ABBREVIATIONS

DO – Dissolved Oxygen

FCC – False Color Composite

FNU – Formazin Nephelometric Unit

NDREI – Normalized Difference Red Edge Index

NGRDI – Normalized Green Red Difference Index

SAV – Submerged Aquatic Vegetation

INTRODUCTION

Upper Potomac

The Potomac River stretches 650 km from its source in western Maryland to its terminus in the Chesapeake Bay and delineates the southern boundary of Maryland. This stretch of the river is divided into four sections: the North Branch Potomac runs from the Fairfax Stone to the confluence of the North and South Branches of the Potomac River, the Upper Potomac runs from the confluence to Harper's Ferry, and the Middle Potomac runs from Harper's Ferry to Great Falls. The final section of the Potomac is the tidal reach, named so because it is affected by the tides of the Chesapeake Bay, and runs from Great Falls to the Chesapeake Bay. A portion of the Upper Potomac near Brunswick, Maryland will be the focus of this study.

The Upper Potomac Basin incorporates 1,600 km^2 of West Virginia, Maryland, and Pennsylvania. Land use associated with the Upper Potomac basin is 69% forest, 22% agriculture, and 1% urban (MD DNR, 2016a). Sediment, nitrogen, and phosphorus loads in the Upper Potomac have been gradually reduced over the last three decades by a concerted effort between multiple states in the Chesapeake Bay watershed to improve the health of the Chesapeake Bay (MD DNR, 2016a). These efforts have reduced the sediment load that reaches the bay from 1,400 metric tons in 1985 to 1,100 tons in 2014, the nitrogen load from 31,750 metric tons in 1985 to 20,400 metric tons in 2014, and the phosphorus load from 2,700 metric tons in 1985 to 1,800 metric tons in 2014 (Moyer et al., 2017). The majority of these pollutants are the result of agriculture in the basin (Moyer et al., 2017). Although the health of the Upper Potomac has been improving in recent years, large amounts of nitrogen and phosphorus are still entering the Potomac and degrading the ecosystem (MD DNR, 2016a).

Submerged Aquatic Vegetation

Submerged aquatic vegetation (SAV) are vascular plants that grow beneath the surface of the water and serve as important ecosystem engineers in fluvial systems. SAV stabilize stream beds and slow water velocity, which increases sediment deposition and nutrient retention, and retains detritus (Carpenter et al., 1986). They increase invertebrate and vertebrate diversity by providing habitat and protection from predators (Flynn et al., 2014). They are a food source for fish, birds, macroinvertebrates, and mammals; they also remove toxins and pollutants from the water (Anker et al., 2014). SAV biomass fluctuates constantly, and these fluctuations impact the chemical environment of fluvial systems. SAV oxygenate water and substrate, and act as nitrogen and phosphorus sinks when growing, but when senescing and dying they release large amounts of nitrogen and phosphorus into the water and their decay consumes large amounts of oxygen (Carpenter et al., 1986).

Many anthropogenic activities, such as agriculture, water diversion, and riparian zone destruction, can alter macrophyte composition (Anker et al., 2014). Increased nutrient availability from agricultural runoff and increased light availability from riparian zone destruction can lead to SAV overgrowth, which can block water flow and increase the likelihood of local flooding and eutrophication (Flynn et al., 2014). Eutrophication often shifts the species assemblage towards fast growing species which decreases species diversity and lowers ecosystem stability (Flynn et al., 2014). These authors suggest that SAV presence and composition can be used as an environmental health barometer which incorporates temperature, light availability, and nutrient load. According to J. Henesey of MD DNR, *Heteranthera dubia* and *Vallisneria americana* are the two dominant species

of SAV in the Potomac in the area near Brunswick and Point of Rocks (personal communication, 4/4/2017).

Benthic Macroalgae

Benthic macroalgae are filamentous macroscopic algae that grow on hard substrate such as gravel or rocks, but they can also grow on SAV as epiphytes (Dean et al., 2015). These algae perform similar ecosystem services as SAV, such as oxygenating water and absorbing nutrients and pollutants, but they are more easily scoured downstream by strong water flow (Davie et al., 2012). These algae can also contribute to eutrophication if water nutrient levels are too high. *Chara sp.*, *Hydrodictyon sp.*, *Cladophora sp.*, *Spirogyra sp.*, and *Rhizoclonium sp.* are eukaryotic benthic macroalgae commonly found in the Potomac (Dean et al., 2015).

Benthic Cyanobacteria

Planktothrix isothrix and *Microseira wollei* (formerly classified as *Lyngbya wollei*) are filamentous cyanobacteria currently found co-occurring with SAV in the Potomac River (MD DNR, 2016b). It is likely that the presence of these cyanobacteria is governed by flow, temperature, and nutrient availability. *P. isothrix* generally blooms in June and July when the river flow slows and water temperature is between 21° and 27°C (MD DNR, 2016b). During these periods growth is likely limited by nutrient availability; nitrogen is abundant in the Potomac, but phosphorus is very low (MD DNR, 2016b). However, *P. isothrix* seems to thrive even when phosphorus is not abundant. It is possible that the benthic nature of both species allows them to obtain phosphorus from the

sediment as has been shown in another benthic cyanobacterium, *Moorea producens* (formerly *Lyngbya majuscula*) (Hanington et al., 2016). It is important to identify these cyanobacteria because it has been reported that some strains produce toxic secondary metabolites that benefit the cyanobacteria by discouraging foraging and combating infection and may contribute to the ability of these species to outcompete other algae in the Potomac (Kurmayer et al., 2016).

Microcystin is one of the secondary metabolites produced by some *P. isothrix*. While *P. isothrix* produces a variety of toxins, microcystin is of particular concern because it is a hepatotoxin that can damage the liver, heart, gills and kidneys (Funari and Testai, 2008). Results of a study on the bioaccumulation and sub-lethal effects of microcystin on aquatic animals by Ferrão-Filho and Kozlowsky-Suzuki (2011) indicate that damage caused by the toxin is generally reversible, but substantial energy is required to detoxify the compound. Sub-lethal doses in macroinvertebrates reduce coordination, inhibit growth, and increase mortality, while chronic exposure to the toxin causes hepatic tumors (Ferrão-Filho et al., 2011). Bioaccumulation of microcystin has been observed in fish, snails, and mussels, and can reach concentrations harmful to humans consuming the contaminated organisms (U.S. EPA, 2015). The poisoning and death of sea otters has been linked to bioaccumulation of microcystin in their invertebrate food sources (Miller et al., 2010). The toxins are released into the surrounding water when cyanobacteria die and microcystin can persist in water for up to three months before biodegrading or being adsorbed onto sediment (Funari and Testai, 2008).

Cyanobacteria blooms can reach levels that yield sufficient toxin to harm or kill mammals that drink the contaminated water (WHO, 1998). The EPA guidelines on

microcystin exposure identify 1 μgL^{-1} as a safe level of the toxin in drinking water. However, the toxicity of microcystin is proportional to the weight of the consuming animal (U.S. EPA, 2015; WHO, 1998). A human health risk assessment of microcystin by Funari and Testai (2008) suggested 0.04 µg kg body $weight^{-1}$ as the limit of safe daily exposure for humans. External exposure in humans can cause skin and eye irritation; when ingested, the toxin attacks the kidneys, brain, and liver (Funari and Testai, 2008). The highest levels of toxicity occur when a bloom collapses naturally or due to treatment, releasing all of the cyanotoxins in the bloom at one time (Paerl et al., 2013). Water samples taken on June 30^{th}, 2017 in the Potomac River near Brunswick, MD found microcystin levels of 0.014 µg L^{-1} as well as 0.003 µg g^{-1} of *P. isothrix* (Hudson and Mattheiss, 2017).

Microcystin is the best studied of the many toxins associated with cyanobacteria, but it is hypothesized that simultaneous exposure to multiple cyanotoxins may increase the detrimental effects on organisms (Funari and Testai, 2008). Funari and Testai (2008) describe several incidences of human exposure to cyanotoxins, the most significant from the treatment of cyanobacteria blooms in a Brazilian reservoir resulting in 2,000 sick and 88 dead among the people who were exposed to the reservoir water. A similar treatment of a reservoir in Australia led to the hospitalization of 150 people (Funari and Testai, 2008).

In local riverine ecosystems, smallmouth bass are used as an indicator of environmental health. A study by Blazer and colleagues (2012) states that 80 to 100 percent of the smallmouth bass in the Potomac are currently intersexed, i.e., individual fish with both male and female reproductive tissue. While still able to reproduce,

fecundity is decreased due to lower sperm quantity and quality (Blazer et al., 2012). Microcystin is a known endocrine disruptor, possibly contributing to the occurrence of intersex in these Potomac fish populations (Rogers et al., 2011).

Mitigation Potential of Remote Sensing

Remote sensing offers an opportunity to frequently and easily assess the vegetation composition of fluvial systems. The SAV and benthic cyanobacteria species assemblages have been established as good measures of ecosystem health (Flynn et al., 2014). While long term daily monitoring may be burdensome, frequent assessment of the autotrophs may lead to a better understanding of natural seasonal fluctuations in these taxa and anthropogenic influences on their distribution (Flynn et al., 2014). Further, remote detection of biomass coupled with field measures of water temperature, flow, and nutrient loading could better define the environmental conditions associated with these potentially harmful blooms. Thereafter, weekly or biweekly remote sensing of fluvial systems could suffice to identify potentially hazardous blooms.

Beaulieu et al. (2013) states that cyanobacteria blooms are common across the United States and will become more common as water temperatures rise. The best means to mitigate cyanobacteria and algae blooms in the Potomac is to reduce nutrient input from agricultural lands around the river and its tributaries (Beaulieu et al., 2013; Dean et al., 2015). Quantitative data on SAV, benthic algae, and benthic cyanobacteria could be used as an indicator of point and non-point sources of excess nutrients. Also, timely and accurate mapping of possibly toxic areas can facilitate treatment, mitigation, or avoidance efforts (Van der Merwe et al., 2015).

Existing Survey Methods

The most common method of estimating SAV and benthic algae is a visual survey either along transects of a specified length and width or with the aid of a quadrat (Anker et al., 2014). Visual surveys are difficult and time-consuming and the resulting data are subjective (Flynn et al., 2014). Remote sensing is another option as high spatial resolution and 3-5 spectral bands have been proven sufficient for species level identification in some terrestrial environments (Anker et al., 2014). Also, depending on the method, remote sensing may be cheaper and easier than visual surveys. Current survey methods are summarized in Table 1.

Table 1: Annotated table of available survey methods for benthic autotrophs in streams and rivers (Alexander et al., 2008; Anker et al., 2014; Van der Merwe et al., 2015; Visser et al., 2013; and Yong et al., 2010).

Method	Advantages	Disadvantages
Visual	• Inexpensive • Flexible scheduling	• Time consuming • Coverage estimates are subjective
Unmanned Aerial Vehicle	• High resolution (1 cm pixel^{-1}) allows differentiation of individual benthic autotrophs • Cheap, fast, and easy • Flexible scheduling	• Very small payload severely limits capabilities of mounted camera • Drones with hyperspectral payload are expensive • Ideal weather required • Short flight time
Manned Aerial Vehicle	• High resolution (0.5 cm pixel^{-1}) allows differentiation of individual benthic autotrophs • Large payload allows mounting of high resolution multispectral or hyperspectral cameras	• Expensive • Requires detailed scheduling • Weather dependent
Free Satellite	• Free • Hyperspectral imagery increases ability to differentiate spectral targets	• Low resolution (30 m pixel^{-1}) does not allow differentiation of individual benthic autotrophs • Weather dependent, cloud cover may obscure area of interest • Satellite path is set, unable to target specific areas
Contract Satellite	• High resolution (30 cm pixel^{-1}) allows differentiation of benthic autotroph communities • Hyperspectral imagery increases ability to differentiate spectral targets • Able to target specific areas	• Expensive • Weather dependent, cloud cover may obscure area of interest

Aerial photography and remote sensing are common methods for quantifying water quality parameters, such as turbidity, chlorophyll *a*, and pollutant concentration over large areas (Gholizadeh et al., 2016). Satellite remote sensing is often used for large lakes, and coastal and oceanic areas, but it does not provide the spatial resolution to accurately differentiate macroalgae species (30 m pixel^{-1}) (Alexander et al., 2008). At a

resolution of 30 m pixel^{-1}, the majority of the Upper Potomac River would be 10 pixels in width, and many of these pixels would be compromised by overhanging vegetation from the river banks. Aerial photography from planes can cover large areas at a higher spatial resolution (0.5 cm pixel^{-1}), but it is expensive and the resolution may still be inadequate for species-level identification of macroalgae and cyanobacteria. Planes and satellites are also susceptible to adverse weather conditions such as cloud cover. Further, it is necessary to schedule plane and satellite coverage ahead of time, which may make it difficult to quickly obtain information on transient cyanobacteria blooms and adds difficulty to planning around adverse weather.

Aerial drones are able to cheaply and quickly provide high resolution images of specific areas (1 cm pixel^{-1}) and have much more manageable logistics. However, they can only carry a light payload, which means they must use a less sophisticated camera than a plane or satellite, and they are only able to cover small areas (e.g., 10,000 m^2 in a 20-minute flight) (Van der Merwe et al., 2015). Aerial drones are restricted to surveying on sunny days with low winds which may limit their usefulness (Alexander et al., 2008). Regardless of the method used, ground-truthing on the same day as the flight is necessary to calibrate collected imagery (Nezlin et al., 2007). It was decided that an aerial drone would be the most efficient method of gathering data for this project because it allows rapid survey of large areas and is able to capture much higher resolution imagery than a plane or satellite.

A study by Flynn et al. (2014) demonstrated the use of an unmanned aerial vehicle (UAV) with a mounted three band Red, Green, Blue (RGB) camera in quantifying the coverage of *Cladophora glomerata* in a shallow non-turbid river. A

visual survey was used to ground truth the remote sensing data and the authors concluded that the digital photography was able to accurately differentiate the filamentous alga from the river substrate. Repeated surveys over the course of a summer captured the seasonal progression of accrual, peak levels, and sloughing of the benthic algae.

Infrared photography is a standard tool for differentiating terrestrial vegetation, and a study by Yong et al. (2010) has demonstrated its ability to differentiate SAV and macroalgae. This author concluded that turbidity and depth are important variables when photographing benthic vegetation. This study also defined some of the limitations of using infrared photography; in particular, water absorbs most wavelengths between 1300 and 2500 nm which limits underwater photography to the near-infrared range of 700 to 1300 nm. This limitation makes vegetation differentiation more difficult in underwater photography than in above water photography, and differentiation was only attempted at the class level (Yong et al., 2010).

Application to the Potomac

The Brunswick portion of the Upper Potomac was an excellent environment in which to test drone remote sensing methods. A several year monitoring project targeting cyanobacteria blooms in the area had recorded baseline occurrence data which allowed this project to target an area that was likely to experience a bloom (MD DNR, 2016b). Additionally, the overall health of Upper Potomac has improved over the previous several decades as efforts were made to reduce nutrient and sediment pollution in the Chesapeake Bay, but cyanobacterial blooms are still common (MD DNR, 2016a). This

area provided a good sample of nutrient pollution-driven cyanobacterial blooms and native SAV targets on which spectral differentiation techniques could be attempted.

Radiometer measurements taken at Point of Rocks indicate that SAV and benthic cyanobacteria in the Brunswick area of the Potomac have consistent and distinct signatures that can be differentiated in the visible and near-infrared range (Figure 1) (M. Tomlinson, personal communication, 9/21/2016). The benthic cyanobacterium *P. isothrix* had higher reflectance values than SAV at approximately 650 nm due to phycocyanin, a unique accessory pigment to cyanobacteria. *M. wollei* also had high reflectance at 650 nm, but it was not as distinctive due to its lower general reflectance relative to SAV. *M. wollei* could be differentiated from SAV and *P. isothrix* more easily at 560 nm or 710 nm.

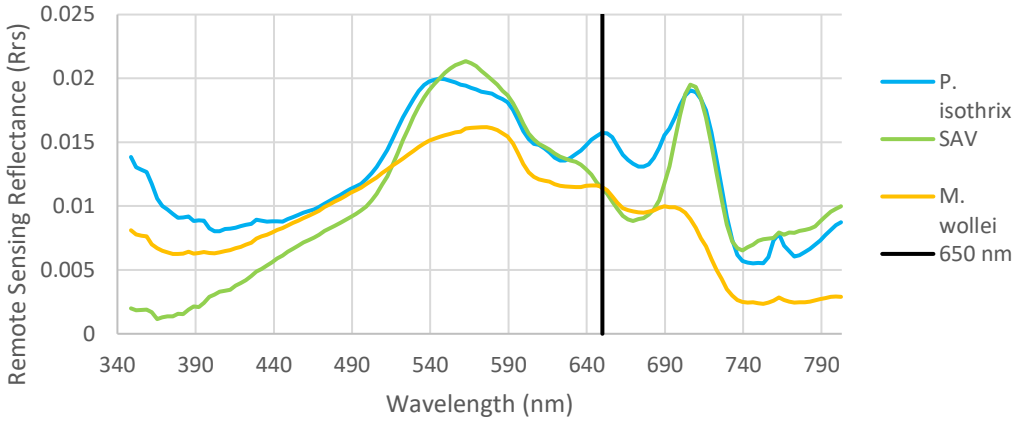

Figure 1: The spectral signatures of the target benthic autotrophs in the Potomac near Brunswick. The vertical black line at 650 nm marks the spike in reflectance associated with phycocyanin.

Digital cameras with high spectral and spatial resolution can capture images in which SAV, substrate, and cyanobacteria can be identified. The ratio of values in each of the captured bands in the digital images should be unique to each autotrophic species, and

each species should be readily identifiable from bottom substrate. The band values associated with each pixel of a delineated species can be used to generate a statistical distribution of values for each band for each species. The difficulty in differentiating species or features is dependent on the uniqueness of the spectral signatures of the targets. Unfortunately, camera equipment that might increase the chance of successful differentiation is prohibitively expensive. If the distribution and ratio of bands is distinct from other species, computer software can identify all other pixels in an image matching that profile.

Project Objective

This study attempted to estimate SAV and benthic cyanobacteria coverage in the Potomac River with a four band, RGB and Infrared, camera mounted on an aerial drone. This study also attempted to differentiate SAV and cyanobacteria to the genus level using the digital spectral data provided in the aerial survey. The objective of this study was to provide methodology for inexpensive and accurate surveys that can be performed quickly to assess benthic autotrophic species composition and an indication of ecosystem health of an area of the Potomac. If successful, use in other shallow water, benthic freshwater systems might be feasible.

METHODS

Survey Equipment

This project utilized both commercially available and custom built survey equipment. Two aerial drones were used, a Phantom 3 quadcopter (registered trademark of DJI Inc., 2017) and a 3DR Solo quadcopter (registered trademark of 3DR Inc., 2017). The Phantom 3 drone was mounted with a Phantom 3 camera. The 3DR Solo was mounted with three different camera configurations: a GoPro Hero 4 Black (registered trademark of GoPro Inc., 2017), a GoPro Hero 4 Black with the fisheye lens and IR filter removed, and a MicaSense RedEdge (registered trademark of MicaSense Inc., 2017) with filters for the default bands. Each drone was capable of approximately 20 minutes of flight time with mounted cameras. Only one camera was mounted for each flight, and several additional batteries were available to allow for multiple drone flights in quick succession. The Phantom 3 and GoPro cameras have identical specifications with varying options for attached lenses. Both cameras can record images in JPEG format, and the Phantom 3 camera can also record in DNG, which is an uncompressed 24-bit format. An annotated list of drone cameras with specifications, advantages, disadvantages, and costs is available in Table 2.

Table 2: Drone mounted camera capabilities and cost.

Camera	Image Quality	Bands	Cost (2017)
GoPro Hero 4 Black	12-megapixel (4,000 x 3,000 pixels) 8-bit JPEG	3-bands (Red, Green, Blue)	$250
Phantom 3 Camera	12-megapixel (4,000 x 3,000 pixels) 8-bit JPEG or 24-bit DNG	3-bands (Red, Green, Blue)	$280
MicaSense RedEdge	1.2-megapixel (1,280 x 960 pixels) 16-bit TIFF	5-bands (Red, Green, Blue, RedEdge, Near-IR)	$4,900

A handheld hyperspectral radiometer (Satlantic Hypergun) was used to collect spectral profiles of the dominant SAV and cyanobacteria taxa in the Brunswick area. M. Tomlinson of NOAA used the Hypergun to capture data from a flat-bottomed boat piloted by J. Henesy of MD DNR; the sensor remained above the water, thereby capturing the target spectra as well as any light attenuation or distortion effects from the water in the Potomac. The Hypergun has a spectral range of 350-800 nm and a spectral resolution of 3.3 nm $pixel^{-1}$. This information was used to identify bands within which the spectral signatures of the target taxa differed the most.

Several pieces of equipment were constructed to aid in data collection and analysis. Kayaks were used to navigate the Potomac during survey and environmental monitoring; all equipment was designed and constructed to operate from a single person kayak. To test the effects of depth, turbidity, and spatial resolution on the cameras used in the survey, a resolution board (Figure 2) was constructed with colors matching the dominant spectral signatures in that area of the Potomac: one substrate color, two SAV colors, and two benthic cyanobacteria colors. A known area of the board was painted in each color and in an increasingly complex pattern of increasingly small squares.

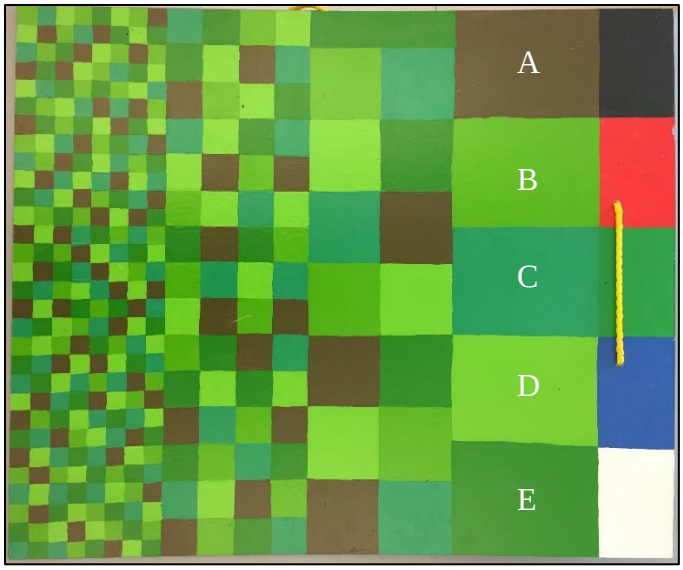

Figure 2: The resolution board placed on the bottom of the Potomac to enable examination of the spatial and spectral resolution of the cameras. From left to right, sizes of rectangles are 2.5 x 2.5 cm, 5 x 5 cm, 10 x 10 cm, and 15 x 20 cm. The black, red, green, blue, and white rectangles on the right edge of the board were included as an attempt to aid in image calibration. The board consists of ½ inch (1.27 cm) plexiglass, painted with latex semi-gloss paint, and covered in a clear matte polyurethane finish. Color A imitates substrate, colors B and C imitate cyanobacteria, and colors D and E imitate SAV.

A floating camera rig (Figure 3) was constructed to maintain a stable platform for the in-water images taken at each control marker (Figure 4). The rig was constructed of PVC, plexiglass, and construction lumber. Two parallel capped tubes of 4-inch (10.16 cm) PVC were used as pontoons, which were connected by two pieces of construction lumber. A ¼-inch (0.635 cm) plexiglass sheet was attached to the boards with industrial Velcro. A 4-inch hole was cut into the center of the plexiglass sheet so that a view tube with a mounted camera could be fitted through the hole. The view tube was constructed from female threaded PVC with a clear acrylic disc glued into the end; the tube was fixed by screwing it onto a male threaded PVC tube through the hole in the plexiglass. The camera mount was taken from the GoPro camera hardware and was fixed with PVC

adhesive. In addition to creating a stable camera platform, the rig held the view-scope just beneath the surface of the water, avoiding distortion from the water surface. The camera rig also allowed an open air connection between the GoPro and an iPhone screen which was necessary for maintaining a Wi-Fi connection between the camera and phone.

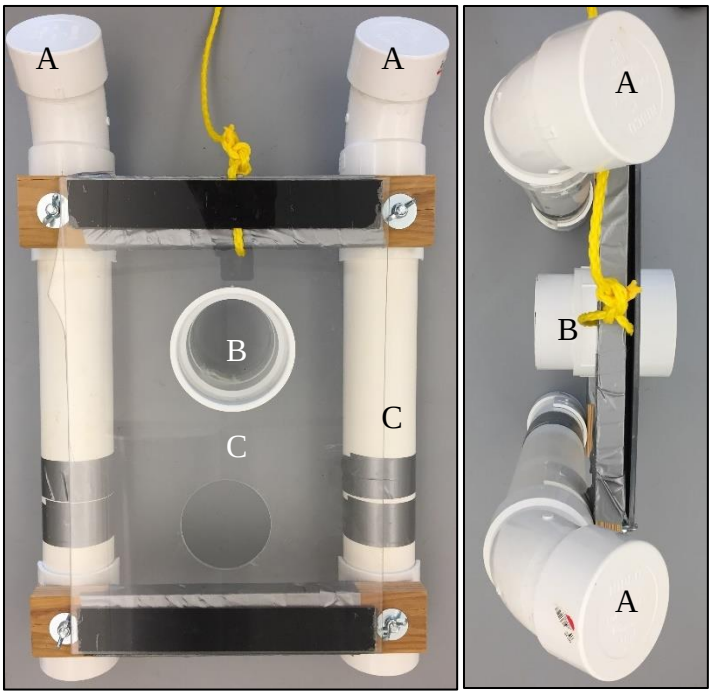

Figure 3: Floating camera rig built to provide a stable platform from which to capture images of locations with georeferenced control markers. Pontoons (A) and view scope (B) were made of plumbing grade PVC, deck (C) was made of ½ inch (1.27 cm) plexiglass and construction lumber, and the GoPro Camera was placed in a GoPro waterproof case and fastened into the view tube and scope with a GoPro Camera mount.

Two-and-a-half-pound (1.13 kg) iron bar weights were spray painted Blaze Orange (Figure 4). After the paint had dried, 5 m lines of 100-pound (45.35 kg) line with 4-inch (10.16 cm) pool floats were attached to each weight. These weights served as control markers that could also be clearly seen in the aerial imagery. The float allowed for them to be quickly located during survey and for easy retrieval afterwards.

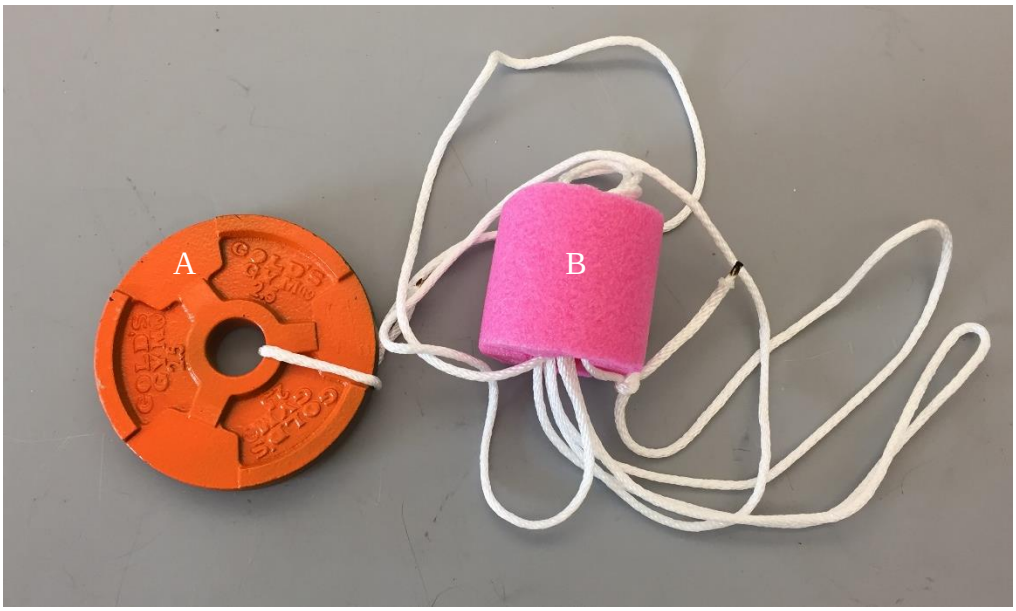

Figure 4: Control markers were placed in the survey area before the drone flights to mark locations that would be used to validate drone imagery, as they were easily spotted from all flight altitudes. The pink float aided in finding the markers from the kayak and was used for retrieval. Markers consisted of 14 cm diameter 2.5 lbs. (1.13 kg) weight (A), painted orange, and attached to a section of pool float (B) by a 5 m length of line.

A scale, to allow length width estimates, was built from a 10-foot length of ¾-inch (1.905 cm) PVC and ¼-inch (0.635 cm) plexiglass. Two 20 x 70 cm sheets of plexiglass were attached so that one end of each completely overlapped creating a right angle (Figure 5). The two 20 x 50 cm portions that did not overlap were then painted in a black and white 10 x 10 cm grid, except for three of the squares, which were painted red, green, and blue. This scale could be attached and detached from a PVC pole by means of a corner bracket and machine screws with wing nuts. The scale was designed to be placed in the view of the camera mounted on the floating rig and held in place with the PVC pole beneath the floating rig until an image had been taken.

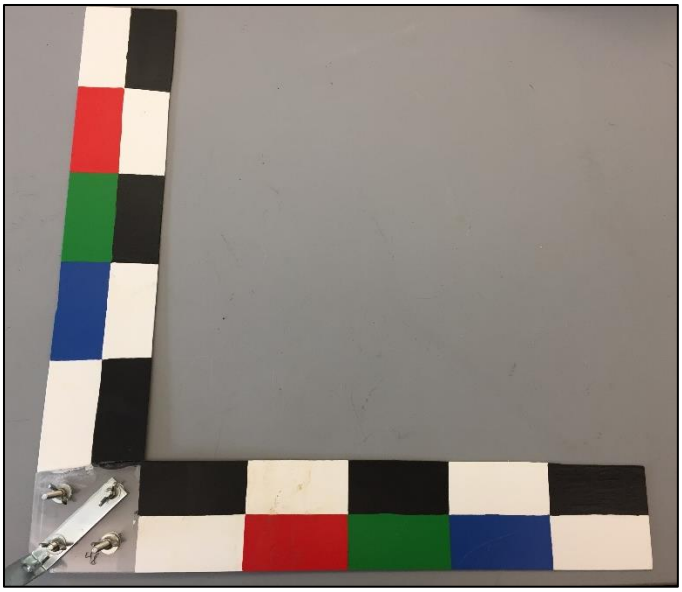

Figure 5: A scale designed to be lowered into the water on the end of a PVC pole and placed adjacent to control markers to give scale and a color palette to control marker images. Painted rectangles are 5 x 10 cm. Scale is built from ¼-inch plexiglass, painted with semi-gloss latex paint, covered in a matte polyurethane finish, and assembled with zinc-coated hardware.

Equipment Efficacy

The survey equipment constructed for the project had mixed success. The resolution test board proved valuable and was able to provide a tangible estimate of camera resolution, as well as a demonstration of the difficulties faced in separating similar colored features with computer software. The orange markers were also very useful. They were easy to deploy and retrieve, did not move while deployed, were clearly visible in the drone images, and the attached floats provided good reference points while navigating between control points on the water.

The floating camera rig was very difficult to maneuver over the control points due to river current; it was much easier to paddle upstream of a marker and slowly float past a marker, capturing the image by hand. The camera rig may prove useful in a lake or pond

where there is little or no current. The graduated scale was used in most of the control point images, but was very time-consuming and difficult to manage in the current. With limited practical use, the project would have moved more efficiently without these constraints.

Preliminary Data Collection

An initial test was performed to determine camera and drone capabilities. Spatial resolution had been cited as the most important variable in attempting species differentiation with digital photography (Anker et al., 2014). Depth and turbidity had been cited as the two most important variables in recording sub-surface water features (Yong et al., 2010). Hence, the resolution board was placed on the ground in an open area and images were recorded with a Phantom 3 camera mounted on a Phantom 3 aerial drone from directly above at altitudes increasing in 5 m increments between 10 m and 50 m. This test was performed to determine the effect of camera altitude and subsequent changes in image resolution on the ability of Terrset software (Clark Labs, 2017) to differentiate and estimate coverage of each of the colors on the board. The results of this test were used to determine the altitude of the aerial drone during the surveys.

An additional experiment was performed to determine the ideal altitude for future surveys because the altitudes identified by the original survey did not provide sufficient resolution. The resolution board and three markers were deployed near the Brunswick boat ramp during a cyanobacteria bloom. The markers and the resolution board were placed approximately 40 m from shore in an area with SAV and some benthic

cyanobacteria. The Phantom 3 drone was used to capture images of the location at 10 m graduated altitudes between 10 and 50 m.

Site Selection

An area near the Brunswick Potomac boat ramp (Figure 6) was selected for the study. The survey area was a 50 x 75 m transect, running north-south near the center of the Potomac, and located 400 m southwest of where US 17 crosses the Potomac south of Brunswick, MD. The survey area was established 70 m south of the northern shoreline to avoid overhanging trees and debris and ensure that the depth was sufficient for a picture to be taken. The survey area was further divided into six 25 x 25 m squares. The drone was launched from a clear area on the western tip of the island immediately south of the Brunswick boat ramp.

The area was chosen for ease of access and because this area had been part of an on-going MD DNR cyanobacteria monitoring project, which had identified cyanobacterial blooms in this location in previous years (J. Henesy, personal communication, 6/27/2017). A USGS flow gauge located at Point of Rocks provided reliable depth and flow data for the Potomac in the survey area. The USGS Little Falls Pump Station, located near Washington, D.C., provided turbidity estimates of the river. Data from the last five years indicated that turbidity was generally low, ranging from 0-10 Formazin Nephelometric Units (FNU), which is considered very clear (USGS, 2017). However, on the days immediately following rain events, turbidity could rise above 300 FNU (USGS, 2017).

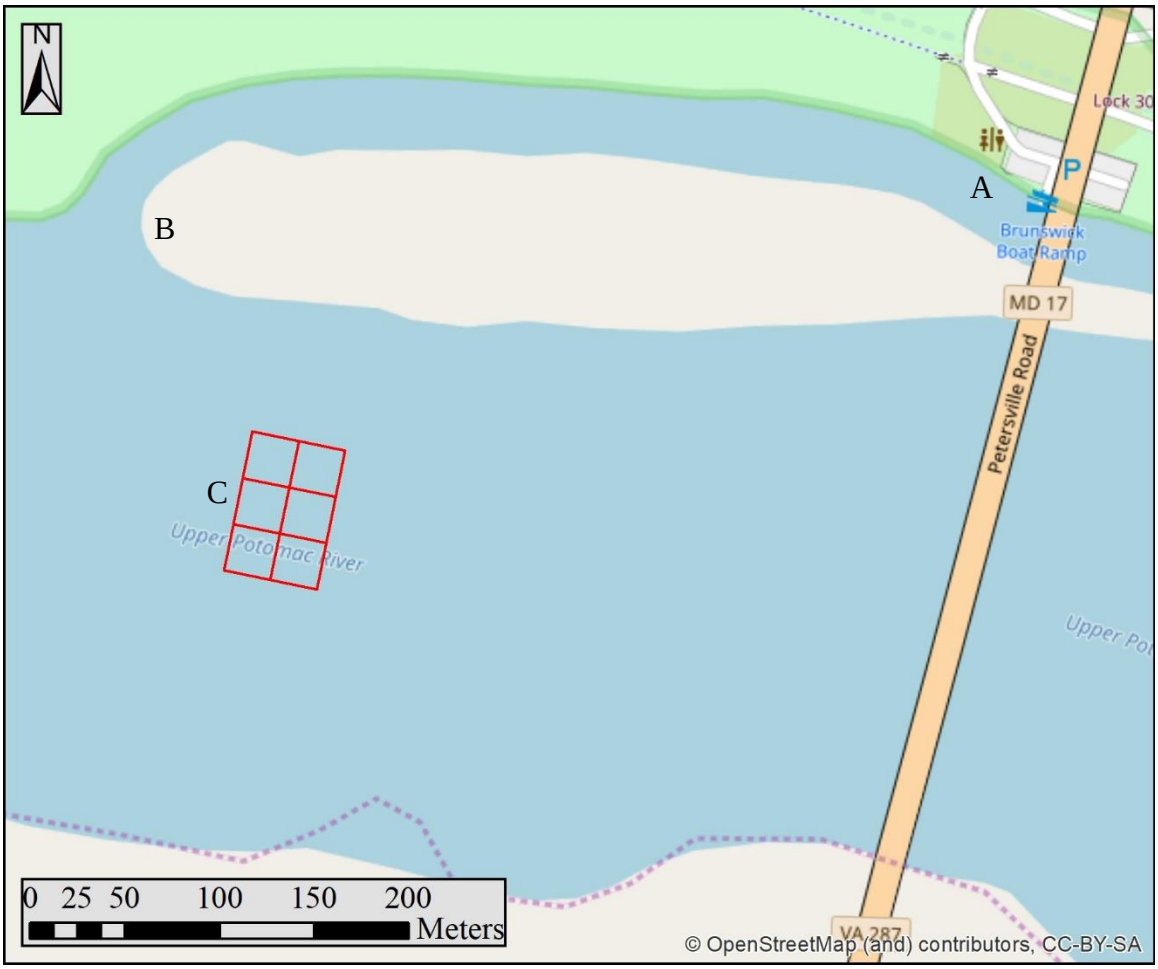

Figure 6: The 50 x 75 m survey area, outlined in red, at Brunswick, MD. Kayaks were launched from the Brunswick Boat Ramp (A). Drones were launched from a clear area on the western tip of the island at the marked location (B). The survey area was divided into a 25 x 25 m grid which was loaded onto a Trimble Juno GPS to aid in marker and board placement (C).

Environmental Monitoring

Constant environmental monitoring was required throughout the field season, May to mid-September 2017. The Brunswick site was visited twice a week and the survey area was inspected for benthic cyanobacteria by kayak. This inspection was not performed if there had been a major rain event or the USGS Point of Rocks flood gauge indicated that the water level and river flow were too high to be safely navigable by

kayak, and a low likelihood of a cyanobacteria bloom. This monitoring strategy ensured that any cyanobacteria blooms formed during the 2017 field season were noted.

When a cyanobacteria bloom was present, water quality and weather forecasts for the survey area were assessed to determine the nearest day most likely to meet the conditions required for aerial survey. During the mid-summer, when it was suspected that water temperatures in the Potomac were too high for a cyanobacterial bloom to occur based on the temperature threshold of 21-27°C observed during previous MD DNR surveys, one survey was conducted to record the SAV present in the survey area. All surveys were conducted under the following conditions: winds less than 4.5 m sec^{-1}, scattered cloud cover or clear skies, no precipitation, a 2°C or greater dew point humidity spread, and a minimum of 1-mile (1.61 km) visibility.

Survey Protocol

The following methods were adopted from studies conducted by Flynn et al. (2014), Levin et al. (2005), Marcus et al. (2008), and Visser et al. (2013). Three survey methods were used to estimate SAV and benthic cyanobacteria abundance: a visual survey, an underwater camera survey, and an aerial drone-mounted camera survey. On each day of survey, temperature, dissolved oxygen (DO) and conductivity were measured with a YSI Multi-Parameter Water Quality Meter at the survey area. After water quality parameters had been recorded, orange control markers with attached floats were placed near the center of each 25 x 25 m square in the survey area. A Trimble Juno GPS loaded with a shape file of the survey area was used to aid in the placement of each marker. Three additional markers were placed in locations with representative examples of one of

the species of SAV or cyanobacteria targeted by the study. Two resolution boards were also placed in the survey area, one in the northeastern and one in the southwestern portion of the site. The drone survey was performed first, after the markers had been placed, and then the visual and camera surveys were performed simultaneously.

The target time for the drone survey was late morning, approximately two hours before solar noon, when the river bottom was illuminated, shadows were reduced, and before the angle of the sun was so high that reflections might obscure the images. The survey consisted of programming two aerial drones to take pictures in a grid across the project area. One drone was a Phantom 3 with a Phantom RGB camera and the other was a 3DR Solo which could be mounted with a GoPro Hero 4 Black RBG IR camera or a MicaSense RedEdge camera. Mission Planner software (Open source software, ArduPilot, 2017) was used to program each drone to undertake flights at two different altitudes, 10 and 50 m. Each flight collected images with 75% longitudinal and lateral coverage. This was necessary to reduce any distortion effects from the camera lens or the water and to ensure enough overlap for the orthomosaic processing software.

The visual survey consisted of visually estimating SAV and benthic cyanobacteria coverage within an approximately 1 m^2 area around each survey marker. After the estimated coverage had been recorded, depth measurements were taken with an electronic depth finder and confirmed with a graduated PVC pole. After these data were recorded, a GoPro Hero 4 Black in a waterproof case was used to capture images of each control marker and surrounding area from just beneath the surface of the water. The GoPro was connected through Wi-Fi to an Apple iPhone 5 in a waterproof case, and the smartphone served as a view screen for the camera. Both surveys were conducted from a kayak.

Images and depth measurements were also recorded for each resolution board. The visual and in-water camera surveys continued until the survey area had been covered or atmospheric conditions made further survey impossible.

Data Processing Protocol

Several computer programs were used to process and analyze the collected imagery. A complete processing protocol with instructions for performing each manipulation is located in Appendix I. Many of the tasks for this project were completed within the free trial window of the following programs.

IBM SPSS 23 (registered trademark of IBM corp., 2013) was used to identify possible correlations between the available environmental data and the observed cyanobacteria blooms. A linear regression was performed to compare water temperatures in the Brunswick area of the Potomac River to water temperatures in the Potomac near Little Falls. Binary logistic regressions were performed using bloom presence or absence by day as the dependent variable and average daily water flow and average daily water temperature as independent variables.

Adobe Lightroom (registered trademark of Adobe Systems Inc., 2017) is image processing software for photographers. It was used to remove lens distortion from images taken with the GoPro camera with the fisheye lens because it has a standard program for correcting the distortions for that specific model camera. This program was also used to convert the 24-bit DNG images taken with the Phantom 3 camera into 16-bit TIFF images that were compatible with ESRI ArcMap (registered trademark of ESRI, 2017) and Terrset IDRISI software.

ArcMap was used to clip aerial images taken from different altitudes to the same spatial extent for comparisons of coverage estimates generated by the methods described below. The images were uploaded as 8-bit JPEG or 16-bit TIFF images and then exported in the same format and bit depth. ArcMap was also used to align each of the five bands captured by the MicaSense camera into the same spatial area.

Pix4D (registered trademark of Pix4D, 2017) is an image processing program designed to create orthomosaics from drone imagery. This program uses the spatial data attached to geotagged images, such as camera altitude, longitude and latitude, and the time stamp to find the relative position of each image. This process orthorectifies images by removing distortions caused by camera angle and altitude, standardizing the perspective and scale of each image. The program then finds matching points in the overlapping areas of each pair of adjacent images; if sufficient matching points are found, the program combines all of the geotagged drone images into one large georeferenced orthomosaic. Pix4D requires high spatial overlap between images and has difficulty finding common points between areas that lack large distinct features which run through multiple images. If successful, the mosaics it generates can be used to analyze large areas.

Drone2Map (registered trademark of ESRI, 2017) is a program that used Pix4D software to orthorectify image sets but has increased compatibility with other ESRI software such as ArcMap. This program was able to create orthomosaics of much higher spatial resolution than the standard Pix4D software. The images captured by the MicaSense RedEdge camera could only be processed by Pix4D or by Drone2Map. The MicaSense camera had five sensors, each filtered to a specific band; each time the camera

recorded an image, it recorded five, one from each sensor. Pix4D and Drone2Map had an algorithm for correcting the distortion caused by the sensors recording from slightly different physical locations on the camera and combined all of the bands into a single image.

Terrset IDRISI (registered trademark of Clark Labs, hereafter referred to as IDRISI) is an image analysis program used to manipulate and analyze individual images as well as orthomosaics. It was used to perform supervised and unsupervised classifications of images and orthomosaics. Parallel piped is a supervised classification method which groups pixels based on training areas. Training areas are user-identified areas of an image that are representative of a feature class. After training areas had been identified, the computer analyzed the pixels within the areas to develop spectral signatures. The Parallel Piped technique places each pixel in an image into the category of whichever spectral signature it most closely resembles. Pixels are left unclassified if they are not represented by any signature. The signatures developed for this project were SAV, Substrate, Marker, and Glare; the processed images were classified into these four categories with the exception of the pixels that did not match any signatures, which were all given null values.

Isocluster is a common unsupervised classification method which assigned pixels to a predetermined number of categories, usually 20, based on how similar the pixels are to each other. Each category contains pixels that are more similar to each other in each available band than they are to pixels in any other category. Using this software, the resulting image was coded into 20 categories which were identified by comparison with the original true color image. These categories, once identified, could be recoded into any

classes desired. This project reclassified the categories into SAV, Substrate, Marker, and Glare. After one of the above processes has been completed, IDRISI was used to estimate the coverage of each of the final discrete categories into an area estimate by multiplying the number of pixels in the category by the area of a single pixel.

IDRISI was also used to create image ratios, which standardize the difference between two bands in each pixel of the image. These image ratios can be useful for separating classes such as vegetation and substrate. The resulting image has one value for each pixel, ranging between -1 and 1, instead of one value for each band for each pixel. These values can be organized into discrete categories by assigning each range of values a unique color. For example, in the Normalized Green Red Difference Index (NGRDI), values below zero are generally substrate or rock while values above zero are generally vegetation.

IDRISI was also used to sample classified images to determine their classification accuracy. Sampling is the standard remote sensing method for testing the accuracy of image classification. The sample function generated a vector file consisting of a stratified random sample of point locations, which were then overlaid on an image. The points were manually classified with the aid of the true color raster image and then compared with the computer-generated classifications of those same point locations. The computer generated an accuracy score based on the number of sample locations correctly classified.

RESULTS

Environmental Monitoring Results

Three cyanobacteria blooms occurred in the Brunswick area of the Potomac between May and September, 2017. The environmental parameters associated with these blooms were consistent with those observed in the MD DNR 2015 Freshwater Fisheries annual performance report (MD DNR, 2016b). Blooms were observed from June 29th to July 6th, August 23rd to 29th, and from September 18th to the end of survey on September 30th. These blooms were observed when Potomac flow was under 5000 ft^3 sec^{-1} (142 m^3 sec^{-1}); other recorded parameters from each day of survey such as water temperature, conductivity, and DO are summarized in Table 3. Figure 7 overlays bloom occurrence on a graph of flow and water temperature data for the 2017 field season from the Point of Rocks USGS Gage[1] Station.

Table 3: Observed environmental parameters at Brunswick on each survey day.

Date	Flow (ft^3 sec^{-1})	Water Temp (C°)	Conductivity (µS cm^{-1})	DO (mg L^{-1})	Bloom
12-Jun	4940	24.3	349	3.6	No
30-Jun	3950	27.4	382.3	2.3	Yes
18-Aug	870	25.5	398	8.3	No
25-Aug	2860	24.7	437.5	9.6	Yes
28-Sep	1500	23.9	529	7.4	Yes

1 Gage is the correct spelling of Gauge in the context of USGS Gage Stations.

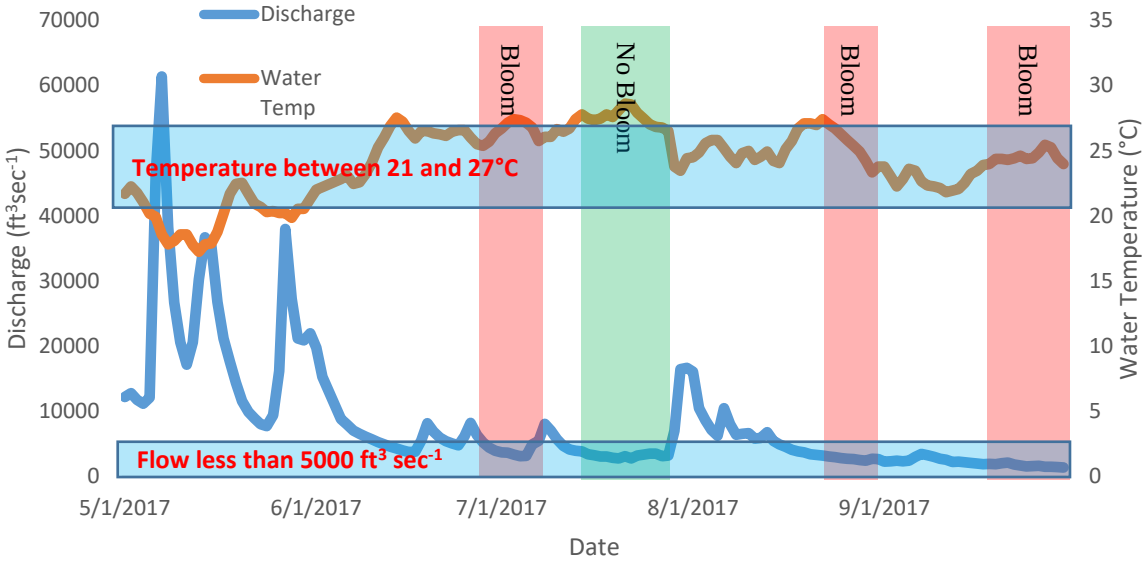

Figure 7: USGS Point of Rocks Gage Station flow data for the 2017 May to October field season (blue), and Brunswick water temperature data (orange). Periods when a cyanobacterial bloom was present in the Brunswick Survey area are highlighted in red. The blue rectangles show the suspected temperature threshold of 21-27°C and the suspected glow threshold of 0-5,000 ft^3 sec^{-1}. It is suspected that there was no bloom during the low flow period in mid-July due to high water temperatures; this period is highlighted in green. It is unknown why the late August bloom ceased and it is unknown why there was no bloom in early September.

The water temperature data used in Figure 7 are based on water temperature data obtained from the USGS Gage Station in Little Falls, D.C., approximately 75 km south of the project area at Brunswick. A linear regression was performed to compare the water temperatures at Brunswick to those at Little Falls water. Forty-one temperature measurements, taken by J. Henesy of MD DNR in the Brunswick area between 2013 and 2016, were compared to the daily average water temperature as recorded by the USGS station at Little Falls. The linear regression indicated that there was a significant relationship ($p < 0.001$ between the daily average temperature at Little Falls and Brunswick. The statistical methods used to justify the validity of the Little Falls daily

water temperature data as a proxy for Brunswick daily water temperature are detailed in Appendix II.

The linear regression generated to analyze the relationship between the water temperatures at Brunswick and Little Falls was also used to transform the Little Falls water temperature for each day when a cyanobacterial bloom was observed in Brunswick. The transformed water temperature data for these 28 days have a mean of 25.3°C, a low of 24.0°C, and a high of 27.4°C. These data closely matched the 21-27°C threshold observed by MD DNR.

A binary logistic regression was performed using average daily flow (recorded at the Point of Rocks USGS Gage Station) and daily average water temperatures (recorded by the USGS Gage Station at Little Falls, D.C.) as independent variables; daily cyanobacterial bloom presence or absence was the dependent variable. Flow and temperature data from the Point of Rocks and Little Falls USGS Flood Gages were obtained from the USGS National Water Information Center website (USGS, 2017). The regression indicated that flow and water temperature were both significantly correlated with the presence or absence of cyanobacterial blooms ($p < 0.002$). The statistical methods used to perform this binary logistic regression are outlined in Appendix II.

This binary regression was repeated seven times; in each regression the independent variables were offset one day further back in time. This was done in an attempt to find possible lagged trends predicting bloom occurrence in the Brunswick area. The statistical significance of the correlation between the independent and dependent variables decreased with each regression. The Hosmer-Lemeshow test, which checks how well the generated model matches the data, was insignificant for the

regressions offset 0, 1, and 2 days indicating that these regressions were valid. The significant Hosmer-Lemeshow tests for the remainder of the regressions indicated that a binary regression is a poor fit for the data. These tests indicated that offsetting the data does not produce valid information and hence, river conditions beyond two days did not affect cyanobacteria in the river.

Binary logistic regressions were used to analyze the data because the dependent variable was a categorical variable consisting of two mutually exclusive categories: bloom and no bloom. If more detailed bloom information is available in the future, such as total benthic cyanobacteria coverage, a multiple linear regression may be more appropriate.

Survey Results

Five surveys were performed but of those five, only three were performed during a cyanobacteria bloom. The first survey was performed on June 12th when there was no SAV or cyanobacteria in the Brunswick portion of the Potomac. This survey was performed to test the methodology proposed for the project. The August 18th survey was performed to gather data on the two dominant SAV taxa while cyanobacteria were absent. The June 30th, August 25th, and September 28th surveys were performed during a cyanobacteria bloom. The drones, cameras, taxa present, and altitudes of the flights specific to each survey date are summarized in Table 4.

Table 4: Survey dates, equipment, altitude, and target taxa presence or absence.

Date	Drone	Camera	Altitude	Target Taxa Present
12-Jun	Phantom 3, DJI Solo	Phantom 3, GoPro Hero 4 Black	10 m, 50 m	none
30-Jun	Phantom 3, DJI Solo	Phantom 3, GoPro Hero 4 Black	10 m, 50 m	*M. wollei*, *P. isothrix*, *H. dubia*, *V. americana*
18-Aug	Phantom 3, DJI Solo	MicaSense RedEdge, GoPro IR	10 m, 50 m	*H. dubia*, *V. americana*
25-Aug	DJI Solo	MicaSense RedEdge	10 m, 50 m	*M. wollei*, *P. isothrix*, *H. dubia*, *V. Americana*
28-Sep	Phantom 3	Phantom 3	10 m, 20 m, 30 m, 40 m, 50 m	*M. wollei*, *P. isothrix*, *H. dubia*, *V. americana*

Data Processing Results

Signature Development

Spectral signatures were developed for *P. isothrix*, SAV, and substrate in images recorded by the GoPro from under the water's surface, the Phantom at 10 m altitude, and the MicaSense RedEdge at 10 m altitude. A signature was not developed for *M. wollei* because it could not be distinguished from the substrate in the images. A Parallel Piped supervised classification was not able to identify the features in the 8-bit images from the Phantom and GoPro, but it was able to identify the majority of the areas of SAV and substrate in the 16-bit MicaSense image. This failure was due to the large amount of variation in the composition of the bottom of the Potomac as well as shadow effects from rocks and SAV.

The signatures are graphed according to band and camera type to demonstrate similarities and differences in the bit values of each pixel (Figures 8 and 9). The GoPro Hero 4 Black and Phantom 3 have the same technical specifications but different lenses; however, the Phantom 3 camera was capturing images from the Phantom 3 aerial drone at an altitude of 10 m and the GoPro was capturing images from just beneath the surface of the water. Both cameras capture images in three bands, Red, Green and Blue; the spectral signature of a target is the statistical distribution of bit values for each of these bands in all pixels identified as belonging to that target. Only three bands are graphed for the 5-band MicaSense RedEdge, Green, Red, and RedEdge, because two of the bands, blue and near-infrared, were of very poor quality.

The box-plots in Figure 8 show the distribution of pixel values associated with the spectral signatures for *P. isothrix*, SAV, and substrate in the three available bands. Each section of the box-plot (bars and shaded rectangles) represents one quarter of the total pixel values. Signatures can be differentiated easiest when there is little overlap between the pixel values of each band and when each target signature has a different ratio of bands. Plots A and B in Figure 8 show that while the three signatures have different band ratios, there is a lot of overlap between the ranges of pixel values. The 10 m Phantom 3 signature in Plot B shows that *P. isothrix* signature can be more easily differentiated from SAV in the Phantom images than in the in-water images. This is demonstrated by the lesser overlap of the pixel values in each band; the *P. isothrix* pixel values are generally higher than the SAV values.

Figure 9 displays the spectral signatures of the target features developed from images captured at 10 m altitude with the MicaSense RedEdge camera. These images

were not compressed and provided 16-bit pixel values as opposed to the 8-bit values of the GoPro and Phantom cameras. This difference in quality means that each pixel has a possible value of 0-65,536 for the 16-bit images as opposed to 0-255 for the 8-bit images. The difference in image quality is apparent in the box-plots in Figure 9, which show much more distinct pixel value ranges than the box-plots in Figure 8. Each signature in Figure 9 also has a distinct band ratio, but if all five of the MicaSense bands were available, the bands would be even more distinct. The combination of more distinct pixel value ranges and distinct band ratios makes the MicaSense camera the better option for differentiating features in the Potomac.

The wide ranges of pixel values for the majority of the bands in each signature are caused by shadow effects and other distortions in the images. For example, the SAV signature includes SAV in full sun and in shadow, new and old growth, damaged and undamaged, and SAV in areas of variable amounts of sun glare off the surface of the water. Each of these variables extends the range of pixel values associated with the signature for each target spectra.

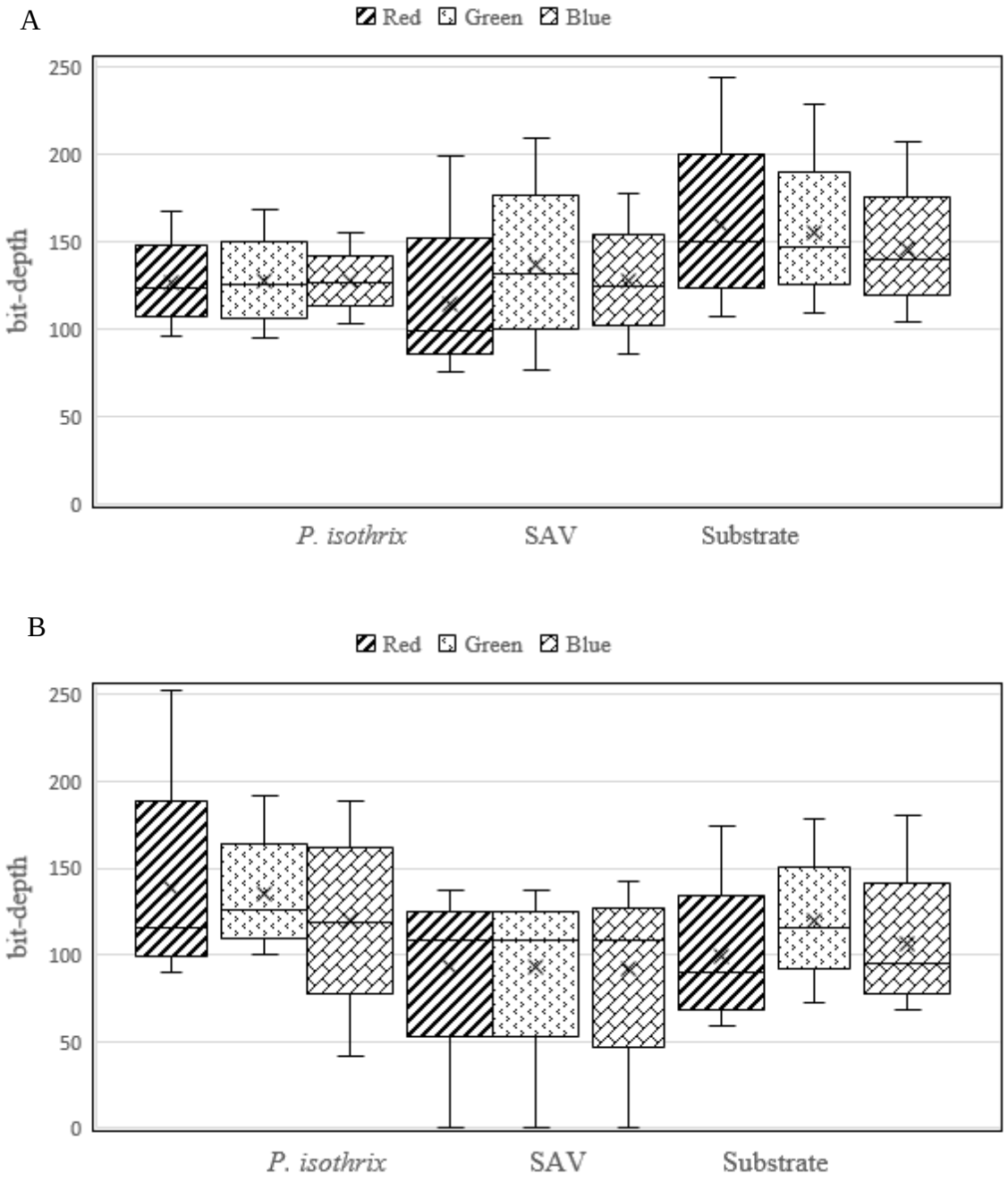

Figure 8: The spectral signatures of the three targets, *P. isothrix*, SAV, and Substrate; these were generated from images captured with the GoPro Hero 4 Black camera (A) from just beneath the surface of the water, and with the Phantom 3 (B) at an altitude of 10 m. The lined box-plots show the signature in the Red band, the dotted box-plots show the signature in the Green band, and the bricked box-plots show the signature in the Blue band. Each of the four sections (bars and shaded rectangles) of each box-plot represent 25% of the pixel values in the signature. The x marks the mean pixel value for each band.

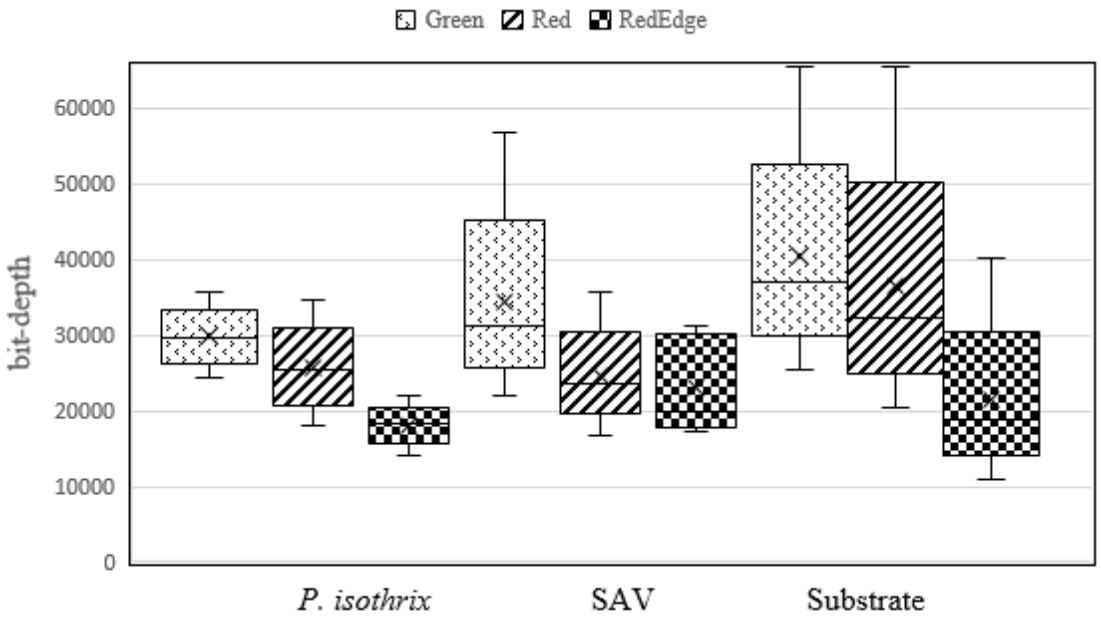

Figure 9: The spectral signatures of the three targets, *P. isothrix*, SAV, and Substrate, generated from an image captured with the MicaSense camera at an altitude of 10 m. The dotted box-plots show the signature in the Green band, the lined box-plots show the signature in the Red band, and the checkered box-plots show the signature in the RedEdge band. The blue and Near IR bands are not graphed because the data from these bands were very poor. Each of the four sections (bars and shaded rectangles) of each box-plot represent 25% of the pixel values in the signature. The x marks the mean pixel value for each band.

Supervised Classification

Figure 10 is a side-by-side comparison of the False Color Composite (FCC) of the Green, Red, and RedEdge bands from the MicaSense Camera, and the result of a Parallel Piped supervised classification. The Parallel Piped classification assigns pixels to categories based on how each band value in each pixel relates to the statistical distribution of each band in the signatures. This procedure was moderately successful for the MicaSense images, but it failed completely when attempted on the GoPro and Phantom images; the transformed images bore little resemblance to the original images, there were no identifiable features. Therefore, only the MicaSense image is shown.

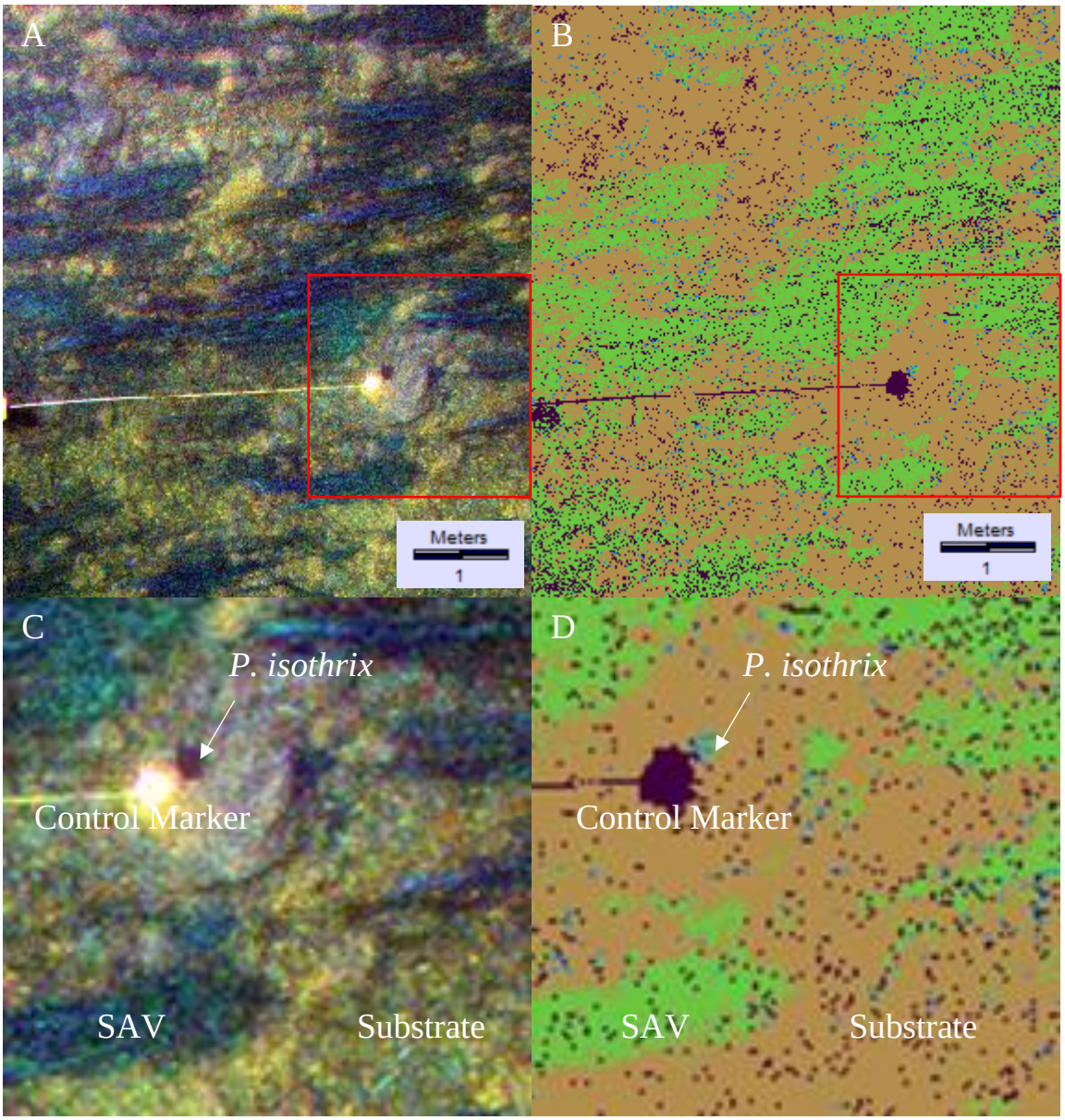

Figure 10: Supervised classification isocluster results. Frame A shows the FCC that is created when the MicaSense bands RedEdge, Green, and Red bands are portrayed as Blue, Green, and Red, respectively. This image was captured from an aerial drone at an altitude of 10 m. Frame B depicts the results of the Parallel Piped supervised classification that classified each pixel according to the spectral signatures of the classes shown in Figure 9. Frames C and D are closer views with labeled features. In the supervised classification, Green corresponds to SAV, blue to cyanobacteria, brown to substrate, and black is undefined.

Unsupervised Classification

Unlike the supervised classification above, an unsupervised classification allows the computer to create its own categories and assign pixels to them in a process called Isocluster Analysis. The program uses pixel values for each band to create a specified number of unique categories and assigns each pixel in the image to the category that it matches most closely. Each generated category is then compared to the original true color image to determine to which of the desired target categories it corresponds (substrate, SAV, *P. isothrix*).

Figure 11 shows the isocluster unsupervised classification result in Panel B and the reclassification of the isocluster output in Panel D. While the 20 categories from the raw isocluster output in Panel B can be difficult to interpret, some patterns are clear. When compared to the true-color image in Panel A, the areas of SAV are distinct from the substrate, the Marker is distinct from both substrate and SAV, and some substrate features such as the large rock near the center of the image are distinct from the surrounding substrate. Unfortunately, the area of *P. isothrix* contains pixel values that are indistinguishable from the areas of SAV. These differences are made clear in Panel D where the isocluster-generated categories have been reclassified into the desired categories of SAV, substrate, and Marker. *P. isothrix* is classified as SAV because it shared similar pixel values, but the SAV and substrate classifications accurately reflect the features in the true color image in Panel C.

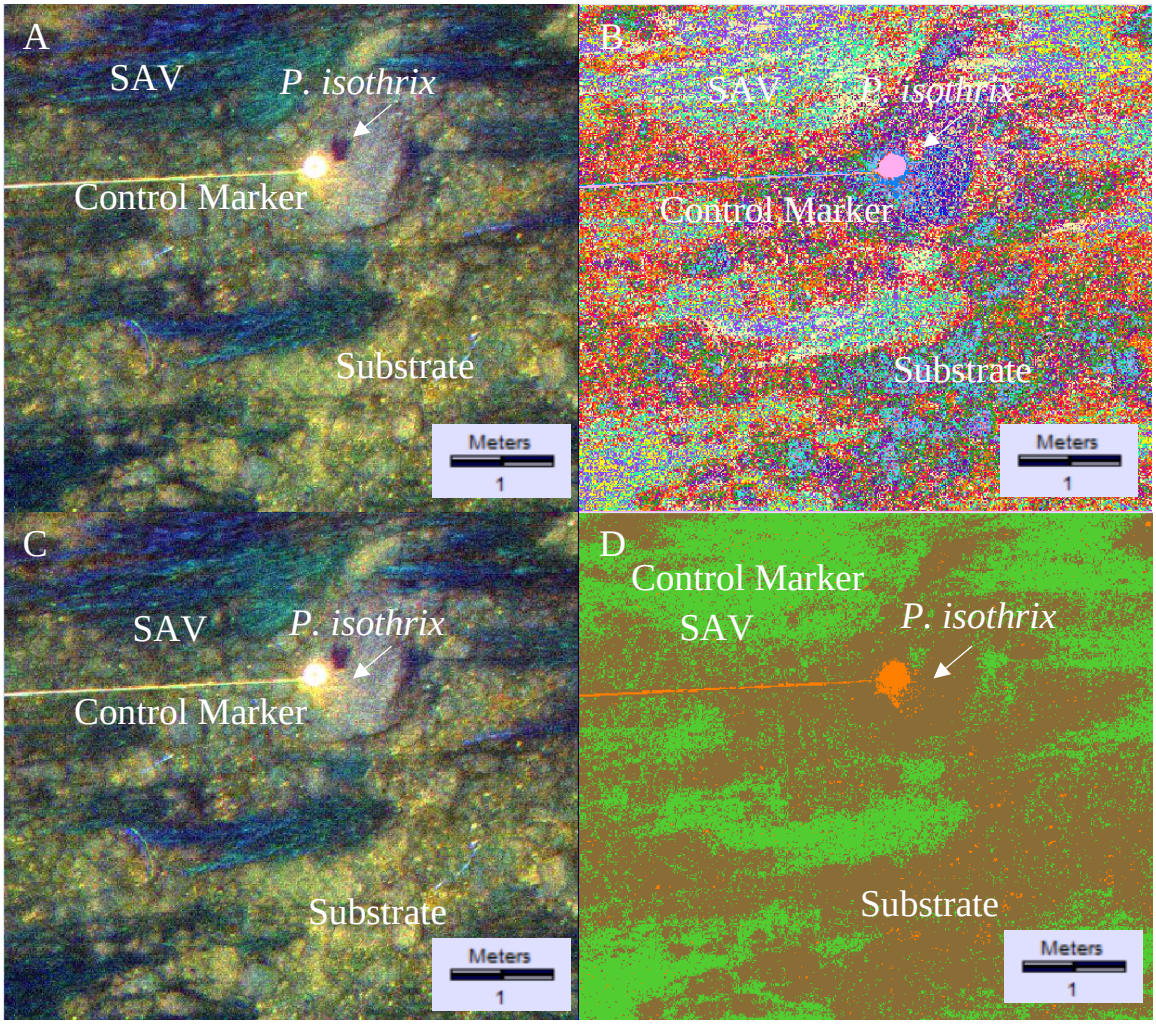

Figure 11: Unsupervised classification isocluster results. Frames A and C portray the FCC created when the MicaSense bands RedEdge, Green, and Red bands are portrayed as Blue, Green, and Red, respectively. This image was captured from an aerial drone at an altitude of 10 m. Frame B shows the results of the isocluster analysis unsupervised classification that assigned each pixel to categories created by the program so that each pixel in each category is more alike to the other pixels in its category than to the pixels in other categories. Frame D is the reclassified isocluster image; each of the 20 classes assigned by the computer was placed into four categories: Substrate, SAV, *P. isothrix*, and Marker. Substrate is brown, SAV is green, and Marker is orange. The analysis was not able to separate *P. isothrix* from SAV.

Image Transformation

The process of transforming images involves mathematically manipulating the values of different bands within each pixel to expose information by simplifying the data

shown in the image. Two image transformations were found to be useful for interpreting the images collected for this project, the Normalized Green Red Difference Index (NGRDI) and the Normalized Difference RedEdge Index (NDREI). The NGRDI formula [(Green – Red) / (Green + Red)] emphasizes the differences between vegetated areas and non-vegetated areas, while reducing shadow and glare effects. The NDREI formula [(RedEdge – Red) / (RedEdge + Red)] also emphasizes the differences between vegetated and non-vegetated areas, but it requires a camera capable of capturing Near Infrared bands.

Figures 12 and 13 show the effects of transforming images with these formulas. Both figures are transformations of the same portion of an image captured with the MicaSense RedEdge camera from an altitude of 10 m. Both transformations were able to utilize the three bands that were effective in the Potomac environment: Green, Red, and RedEdge. After the formula had been calculated, a point near zero was chosen as the dividing line between substrate and vegetation. The FCC of the original image was used to aid in this process. All pixels containing a value below the dividing line were classified as substrate, and all values above the line were classified as vegetation. Of the two methods, NDREI has better feature definition. Neither transformation was able to distinguish between benthic cyanobacteria and SAV, but their ability to distinguish benthic autotrophs from substrate was tested by sampling the images (Figure 14).

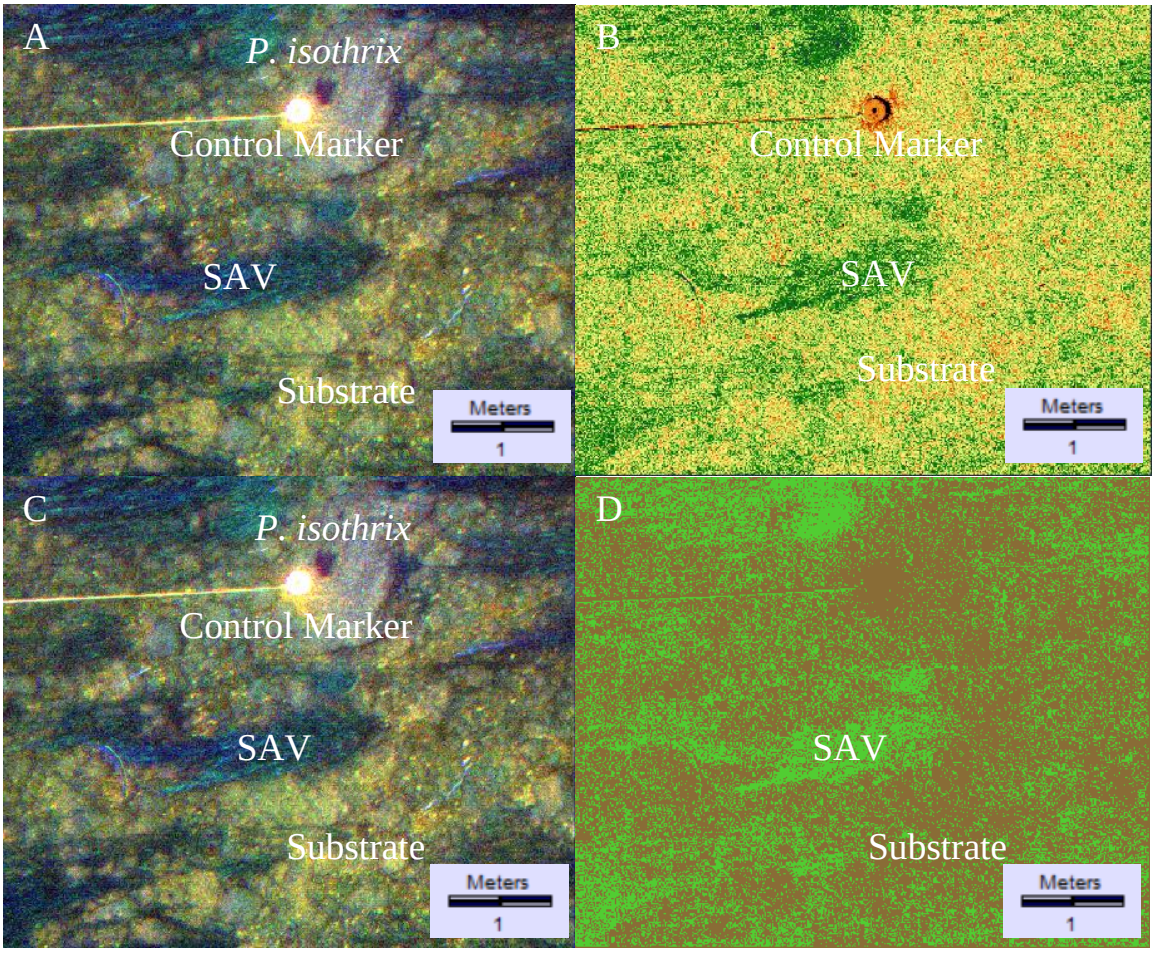

Figure 12: Normalized Green Red Difference Index transformation results. Frames A and C show the FCC created when the MicaSense bands RedEdge, Green, and Red bands are portrayed as Blue, Green, and Red, respectively. This image was captured from an aerial drone at an altitude of 10 m. Frame B shows the process of transforming a 16-bit MicaSense image with a NGRDI formula. Pixel values in the image range from -1 to 1 but the contrast has been adjusted to display the greatest amount of information. Positive values are on the green side of the scale and show vegetation. Negative values are on the red side of the scale and show substrate. Frame D shows the same transformation after the values have been simplified further into a binary distinction between vegetation and substrate. Substrate is shown in brown and vegetation is shown in green. This transformation was useful for obtaining quantitative coverage estimates of benthic autotroph and substrate, but this transformation was unable to differentiate SAV from cyanobacteria.

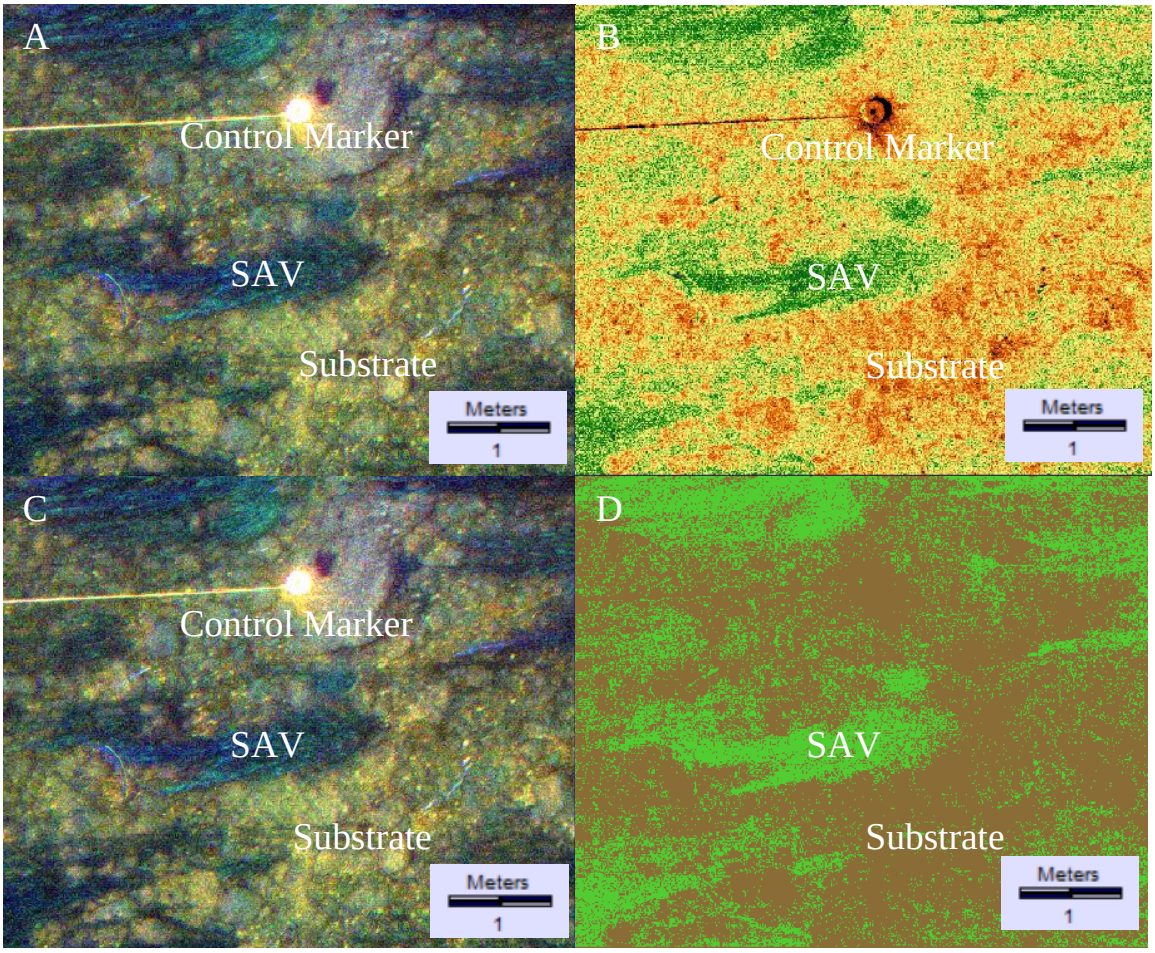

Figure 13: Normalized Difference Red Edge Index transformation results. Frame A and C show the FCC created when the MicaSense bands RedEdge, Green, and Red bands are portrayed as Blue, Green, and Red, respectively. This image was captured from an aerial drone at an altitude of 10 m. Frame B shows the process of transforming a 16-bit MicaSense image with a NDREI formula. Pixel values in the image range from -1 to 1 but the contrast has been adjusted to display the greatest amount of information. Positive values are on the green side of the scale and show vegetation. Negative values are on the red side of the scale and show substrate. Frame D shows the same transformation after the values have been simplified further into a binary distinction between vegetation and substrate. Substrate is shown in brown and vegetation is shown in green. This transformation was useful for obtaining quantitative coverage estimates of benthic autotroph and substrate, but a lot of information was lost in the transformation process. This transformation was unable to differentiate SAV from cyanobacteria.

Accuracy Assessment

The accuracy of each of the feature classification methods shown in Figures 10-13 was tested with Terrset IDRISI, which provides dedicated accuracy assessment programs. A stratified random sample of 50 pixels was generated for the image as a vector file which was then overlaid on the original FCC (Figure 14). Each sample location was manually assigned to a category, which the computer then compared to the classified image. An error matrix was generated which showed how well each category was defined based on how many of the sample pixels were correctly classified. The accuracy assessments of the classification methods attempted in Figures 10 - 13 are shown in Table 5.

The accuracy of the various classification methods varied from 48% to 64%; the percent is the proportion of correctly classified pixels. The Parallel Piped supervised classification correctly classified 48% of the pixels, the isocluster unsupervised classification correctly classified 62%, the NGRDI correctly classified 52% and the NDREI correctly classified 64%. The majority of the error in each of the four classification methods was caused by an overestimation of SAV coverage.

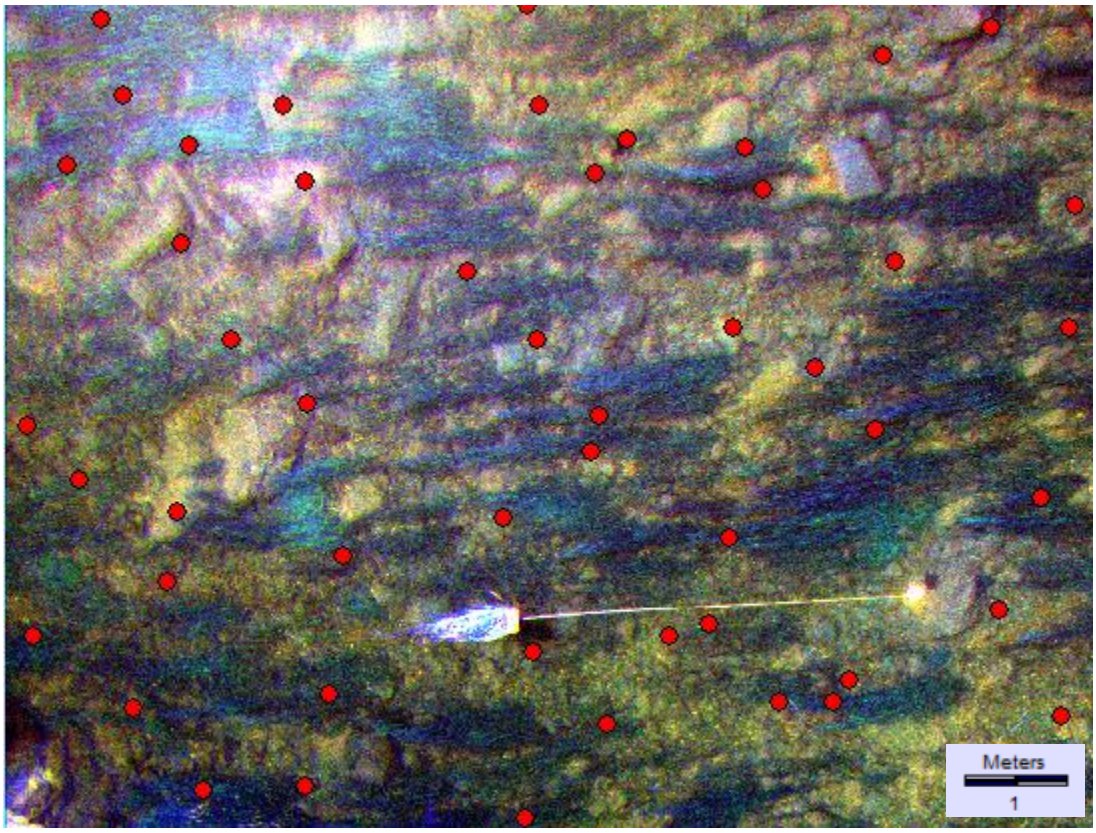

Figure 14: Sample locations for accuracy assessment. Red dots mark the stratified random sample locations generated for the accuracy assessment. Each location was manually assigned a category. The manually assigned categories for the sample pixels were then compared with the results of the classification methods for the sample pixels to generate an error matrix of correctly and incorrectly identified cells.

Table 5: Summary of classification error matrices for the attempted classification methods. The rows are the mapped category values and the columns are the true values of the sample locations. Cells at the intersection of identical row and column headings were correctly identified, other cell values were misidentified. The Accuracy column shows the percent of the sample points that were correctly categorized by each method.

Parallel Piped Supervised Classification			
	Substrate	SAV	Accuracy
None	3	3	
Substrate	12	16	
SAV	4	12	48%
P. isothrix	0	0	

Isocluster Unsupervised Classification			
	Substrate	SAV	Accuracy
Substrate	14	13	
SAV	5	17	62%
Marker	0	1	

NGRDI Image Transformation			
	Substrate	SAV	Accuracy
Substrate	15	20	52%
SAV	4	11	

NDREI Image Transformation			
	Substrate	SAV	Accuracy
Substrate	15	14	64%
SAV	4	17	

Orthomosaics

Orthorectification was attempted with several different programs for each altitude and camera used in each day of survey. Figures 15, 16, and 17 show the orthomosaics generated with Drone2Map from the Phantom 3 June 30th 10 and 50 m altitude image sets and Pix4d from the MicaSense August 18th 50 m altitude image set. Only three of the five MicaSense camera bands, Green, Red, and RedEdge, collected usable data, while Blue and Near Infrared did not. The MicaSense mosaic shown in Figure 15 is an FCC with RedEdge, Green, and Red in the Blue, Green, and Red bands, respectively. All images were captured in the same survey area; however, the total area covered by each mosaic differs considerably due to different environmental conditions, pilot errors, and other delays affecting battery life and image quality.

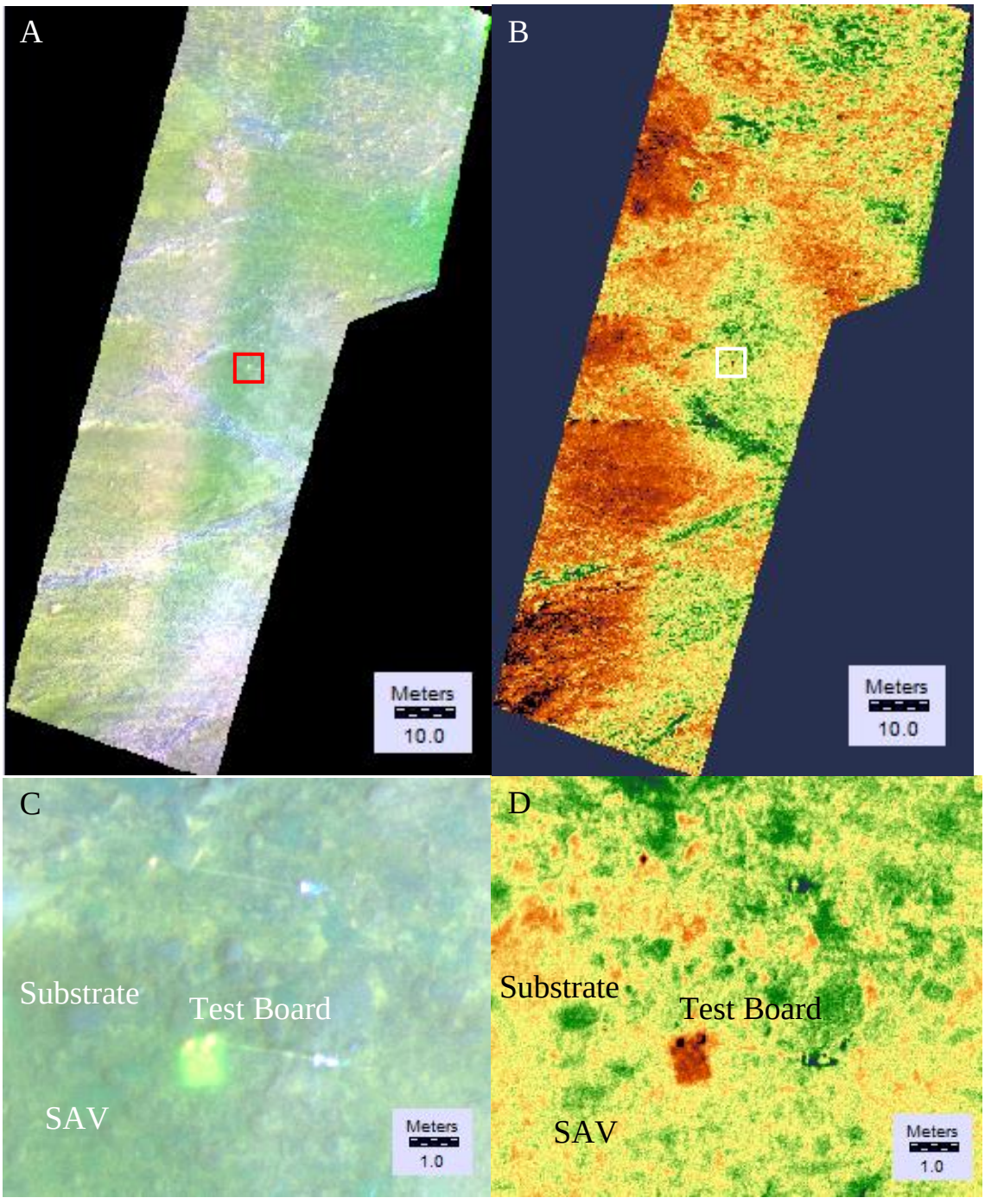

Figure 15: August 18th 50 m MicaSense orthomosaic and NDREI. Frame A shows the FCC orthomosaic created when the MicaSense bands RedEdge, Green, and Red bands are portrayed as Blue, Green, and Red, respectively for the image set captured on August 18th at an altitude of 50 m. Frame B shows the results of the NDREI transformation of the orthomosaic. Frames C and D are closer views of the outlined areas of Frames A and B with labeled features.

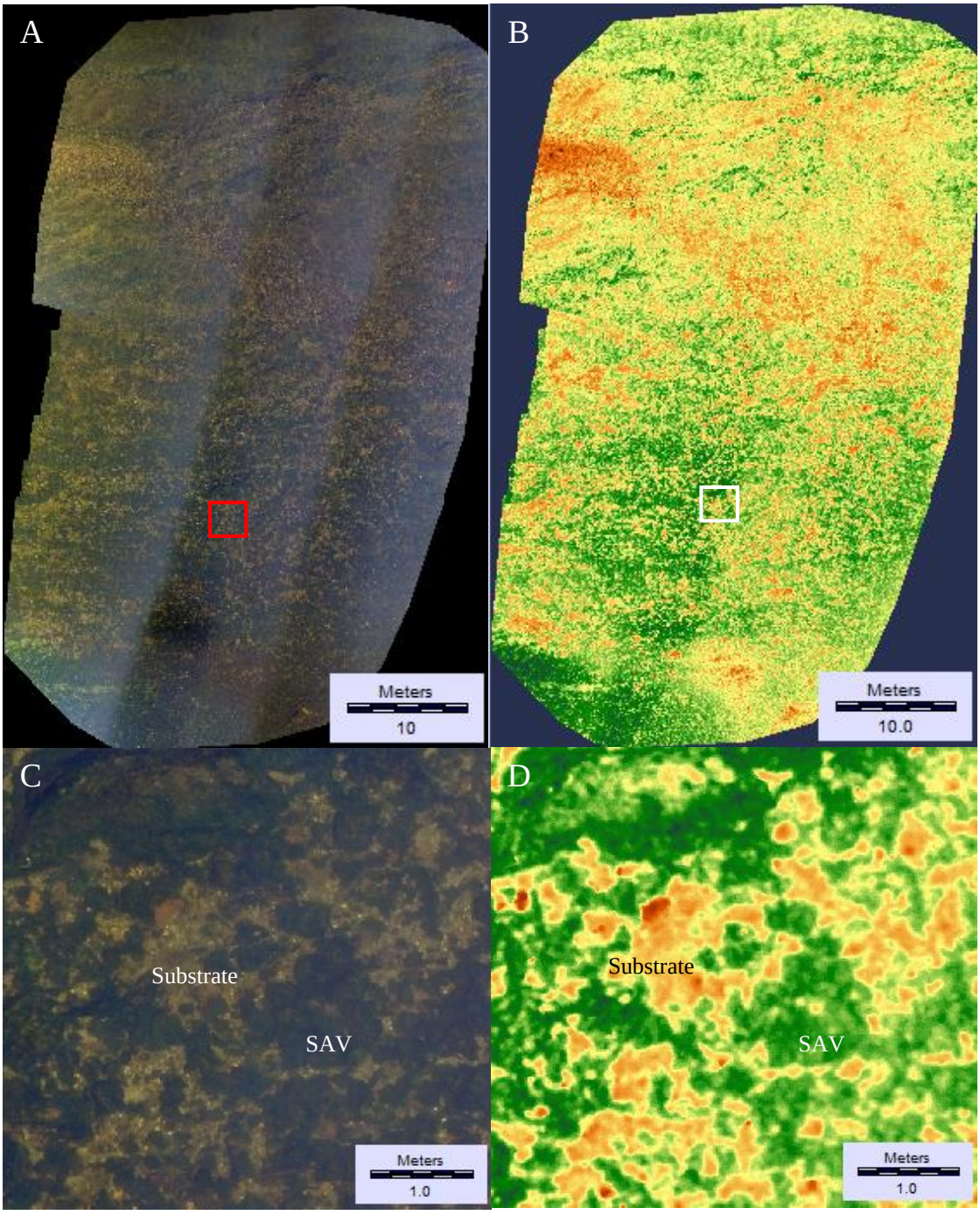

Figure 16: June 30th 10 m Phantom 3 orthomosaic and NGRDI transformation. Frame A shows the true color orthomosaic created from the image set captured with the Phantom 3 Camera on June 30th at an altitude of 10 m. Frame B shows the results of the NGRDI transformation of the orthomosaic. Frames C and D are closer views of the outlined areas of Frames A and B with labeled features.

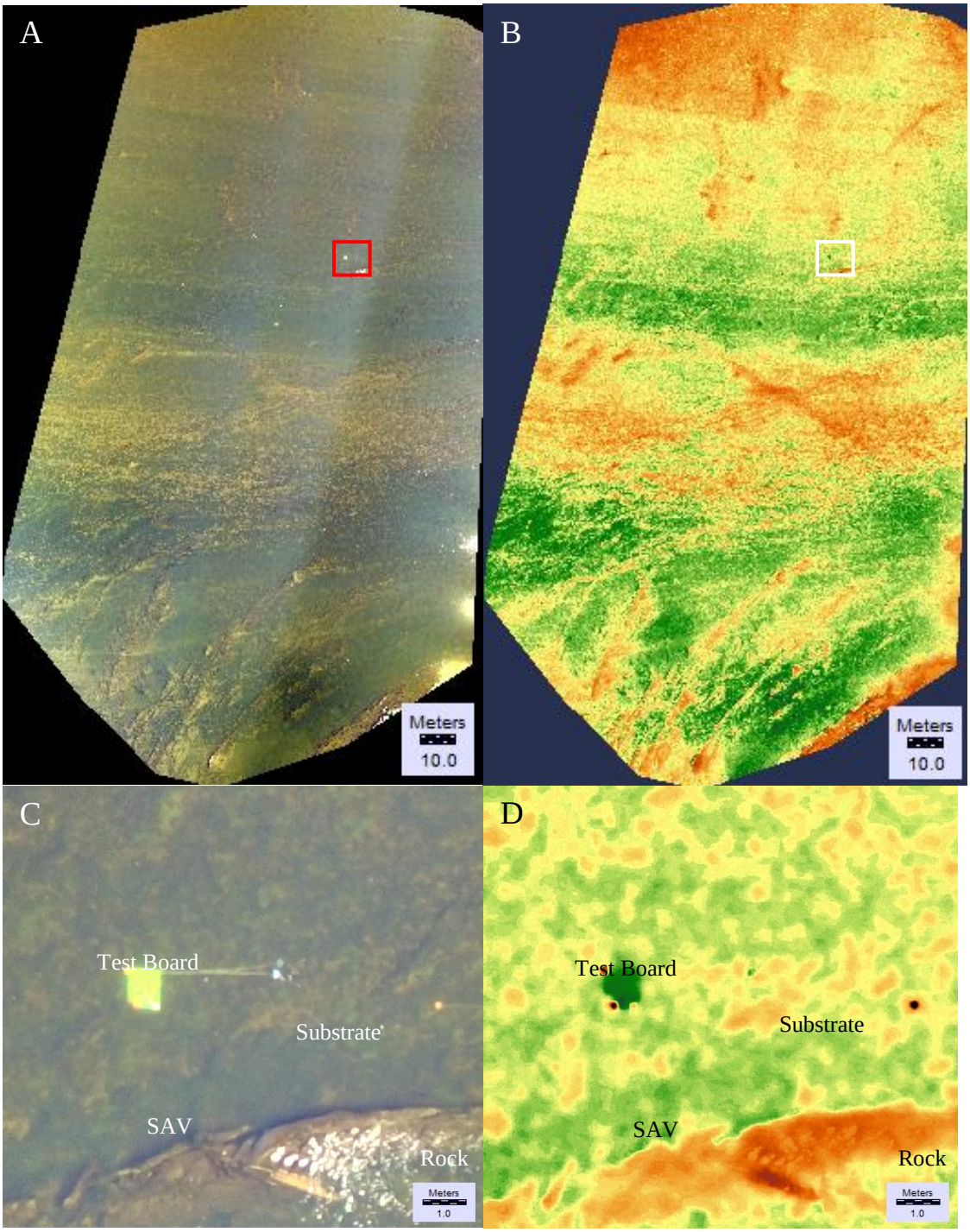

Figure 17: June 30th 50 m Phantom 3 orthomosaic and NGRDI transformation. Frame A shows the true color orthomosaic created from the image set captured with the Phantom 3 Camera on June 30th at an altitude of 50 m. Frame B shows the results of the NGRDI transformation of the orthomosaic. Frames C and D are closer views of the outlined areas of Frames A and B with labeled features.

The linear discolorations running through each orthomosaic are relics of sun glare. High overlap between images, 70 to 80 percent, is necessary for the orthomosaic process. After the images had been standardized to remove slight variations in camera altitude and angle, the pixel values in areas of overlap were averaged to smooth the transition from image to image. However, all of the surveys for this project were performed later in the day than had been planned, and the higher sun angle resulted in sections of glare in each image. As the glare was in the southeastern portion of each image, long streaks of brighter pixels were created in the orthomosaic. The glare issue was more pronounced in the 10 m than in the 50 m altitude flights because at the lower altitude, a greater portion of each image was glare.

These streaks confounded attempts at supervised and unsupervised classifications because there were many different spectral signatures for each target. Signatures were developed for both glare and non-glare portions of targets, but there was too much overlap in the resulting signatures to accurately classify the images. The unsupervised classification failed because the areas of glare exaggerated the range of pixel values so that different targets within an area of glare were more alike to each other than the same target in non-glare areas.

The glare issue was partially resolved by using the normalized difference transformations in the orthomosaics shown in Figures 15-17. In an image with few shadows and uniform lighting, a Red Green Difference Index, [Green – Red] would be sufficient to expose the differences between vegetation and substrate. Images from the Potomac had substantial glare and shadow effects and the lighting sometimes changed between shots as environmental conditions shifted. The NGDRI was able to reduce or

resolve light and shadow effects by standardizing the difference, [(Green – Red) / (Green + Red)], making each pixel value a ratio of the Green Red difference to its total Red and Green. As can be seen in Figures 16 and 17, this method greatly reduced distortion from light effects, but it was much less successful when applied to the MicaSense image orthomosaic in Figure 15.

Relationship between Altitude and Image Resolution

The GoPro Hero 4 Black and the Phantom 3 camera were both 12 megapixel cameras, meaning they recorded 3,000 x 4,000 pixel images. This camera resolution was standard for drone-mounted cameras as a compromise between technical ability and weight. As camera altitude increased, more ground area was captured in each image, but image resolution decreased. A resolution board was created and placed on the bottom of the Potomac before each survey so that it was captured during the programed flights. The resolution test board provided a way to find the size of the smallest area that could be differentiated from the surrounding area at each altitude.

Spectral resolution was tested by cropping the test board out of the surrounding environment in images taken at different altitudes and running an isocluster analysis. The resulting image demonstrated the ability of the program to differentiate similar colors at different levels of spatial complexity. The isocluster image was reclassified to more closely reflect the colors found on the actual board to aid in interpretation. The spatial resolution was tested by the increasing spatial complexity of the resolution board across its length. As the camera altitude increased, the proportion of pixels that contained information from two or more of the colors on the resolution board to the pixels that only

contain information from a single color on the resolution board increased. This had the effect of averaging the spectral characteristics of the different colors in the pixels that overlap multiple categories. The program was then unable to differentiate the colors because the pixel values formed a smooth curve instead of distinct groups.

Figure 18 shows the resolution board as it was captured by the Phantom 3 camera at altitudes of 10, 30, and 50 m. Only the images from the 10 m altitude flight were able to differentiate most of the 6.25 cm^2 squares, while some of the squares with similar colors were muddled. The program was unable to classify any of the sections of the 50 m altitude image of the resolution board. Decreasing image resolution quickly decreases the ability of the image analysis software to distinguish similar spectra. It is important to note that the human eye can distinguish the different colored squares much better than the computer.

The compromise between area coverage and image resolution was central to this project. Most of the SAV present in the survey area covered sufficient bottom area that each individual plant could be distinguished at an altitude of 50 m. However, growths of *P. isothrix* and *M. wollei* varied greatly in the area they covered: the smallest patches were about 5 cm^2 while the larger patches carpeted the substrate. The cameras used for the survey did not possess the spectral resolution necessary to differentiate benthic cyanobacteria from the SAV and substrate. Therefore, the remainder of the results will focus on the accuracy of the total benthic autotroph coverage that could be differentiated from the substrate both spatially and spectrally with the available data.

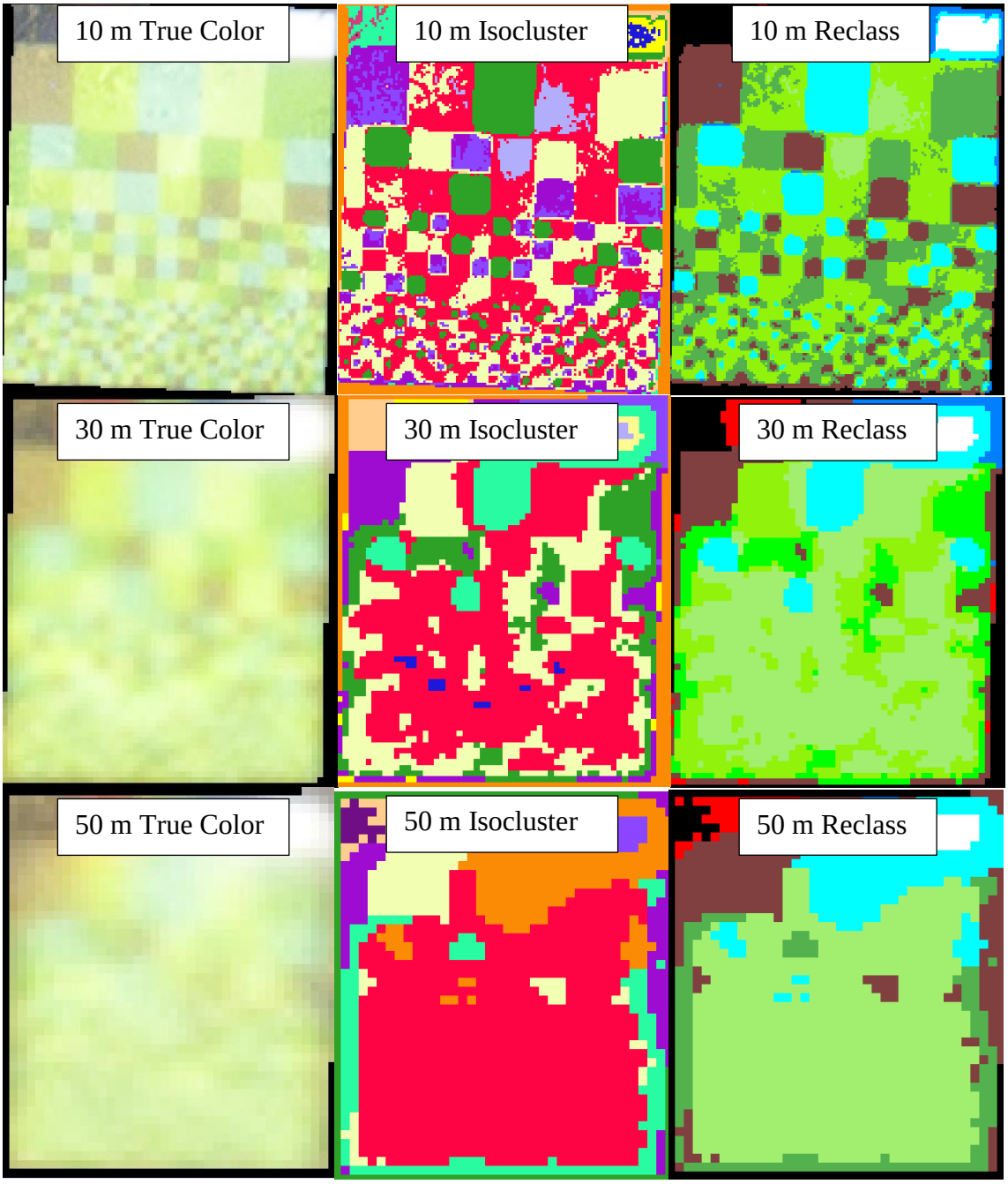

Figure 18: Resolution board captured from different altitudes. The images demonstrate the effect of image resolution on the ability of the unsupervised classification to distinguish unique spectra. The left column is the true color images of the resolution board cropped from the aerial images. The middle is the isocluster analysis result and the right is a reclassification of the isocluster into more identifiable colors. Decreasing image resolution quickly decreases the ability of the image analysis software to distinguish similar spectra.

Effect of Camera Altitude on Vegetation Coverage Estimates

The effect of camera altitude and the resulting image resolution on the vegetation and substrate coverage estimates of the unsupervised isocluster analysis and NGRDI transformation was tested using the sampling strategy shown in Figure 14. Five images were captured in an area near the Brunswick boat ramp at altitudes of 10, 20, 30, 40, and 50 m; the images were then clipped to cover an identical spatial area. The images were captured during a cyanobacteria bloom; living *P. isothrix*, senescing *P. isothrix*, SAV, and substrate along with the resolution board and three markers were within the chosen spatial extent.

The isocluster analysis and NGRDI images for each altitude were each tested with 50 sample locations; the resulting 10 classification error tables are shown in Table 6. Camera altitude did not seem to have an effect on the estimate accuracy of each method within the range of altitudes tested. The error analysis indicates that the NGRDI is a more accurate representation of autotroph and substrate than the isocluster analysis. However, the results were confounded by the senescing cyanobacteria, which covered much of the substrate and SAV in the survey area. The senescing cyanobacteria was spectrally unique in the isocluster analysis and received its own class while apparently actively growing *P. isothrix* was classified as SAV. In the binary NGRDI classification, senescing *P. isothrix* was classified as substrate while living cyanobacteria was classified as SAV (Figure 19).

Table 6: Summary of classification error matrices of the isocluster analysis and NGRDI transformation of Phantom 3 images captured at altitudes of 10, 20, 30, 40, and 50 m. The error analysis indicates that altitude does not have a large effect on classification accuracy at the attempted altitudes. The NGRDI seems to be the more accurate of the two methods but the transformation classified living *P. isothrix* as SAV and senescing *P. isothrix* as substrate, whereas the isocluster analysis classified living *P. isothrix* as SAV and differentiated between senescing *P. isothrix* and substrate.

10 m Isocluster						10 m NGRDI		
	Substrate	SAV	Marker	Senescing	Accuracy	Substrate	SAV	Accuracy
Substrate	0	0	0	2		32	11	76%
SAV	1	7	0	4	58%	1	6	
Marker	0	0	1	0				
Senescing	5	9	0	21				
20 m Isocluster						20 m NGRDI		
	Substrate	SAV	Marker	Senescing	Accuracy	Substrate	SAV	Accuracy
Substrate	0	0	0	1		34	7	86%
SAV	0	12	0	4	78%	0	9	
Marker	0	0	0	0				
Senescing	2	4	0	27				
30 m Isocluster						30 m NGRDI		
	Substrate	SAV	Marker	Senescing	Accuracy	Substrate	SAV	Accuracy
Substrate	1	0	0	2		26	16	64%
SAV	0	8	0	3	60%	2	6	
Marker	0	0	0	0				
Senescing	1	14	0	21				
40 m Isocluster						40 m NGRDI		
	Substrate	SAV	Marker	Senescing	Accuracy	Substrate	SAV	Accuracy
Substrate	0	1	0	1		28	12	72%
SAV	0	12	0	0	74%	2	8	
Marker	0	0	0	1				
Senescing	3	7	0	25				
50 m Isocluster						50 m NGRDI		
	Substrate	SAV	Marker	Senescing	Accuracy	Substrate	SAV	Accuracy
Substrate	0	4	0	0		27	15	66%
SAV	0	4	0	0	56%	2	6	
Marker	0	0	0	0				
Senescing	4	14	0	24				

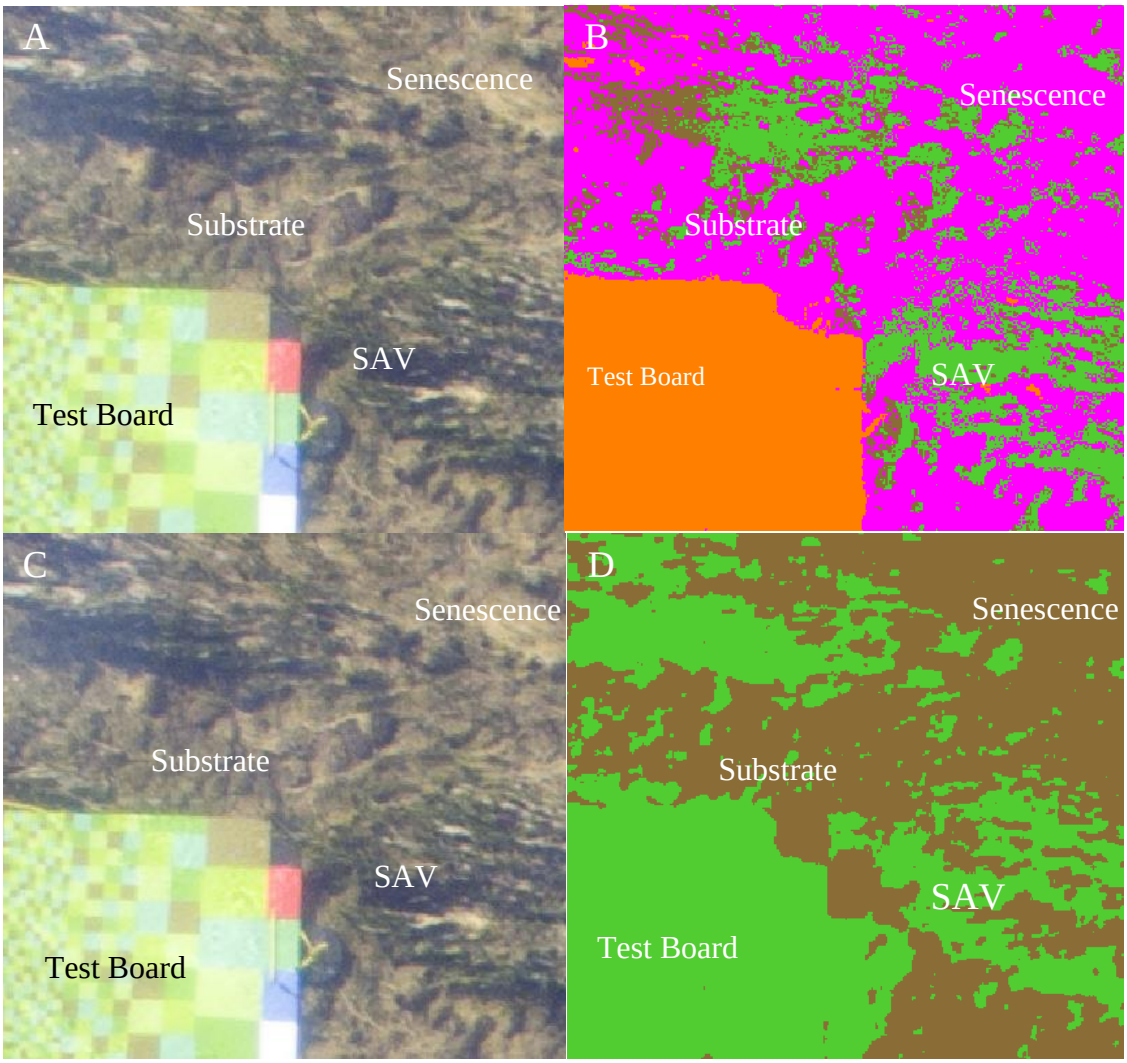

Figure 19: 10 m Isocluster Analysis and NRGDI of senescing *P. isothrix* bloom. Frames A and C show the true color image captured with the Phantom 3 Camera at an altitude of 10 m. Frame B shows the reclassified isocluster analysis: brown is substrate, green is SAV, pink is senescing *P. isothrix*, and orange is the resolution board. Frame D shows the results of the reclassified NGRDI transformation: brown is substrate and senescing *P. isothrix*, green is SAV. Of special note is the way *P. isothrix* covers substrate and SAV. In the top right image (B), shadow is misclassified as substrate and substrate is misclassified as senescing *P. isothrix*.

DISCUSSION

Environmental Monitoring Discussion

The environmental monitoring strategy of twice-a-week visits to the project area combined with input from weather stations and USGS Gage Stations seems to have been sufficient for noting every cyanobacterial bloom between the beginning of June to the end of September, 2017. Binary logistic regression was performed using flow data from the USGS Gage Station at Point of Rocks and water temperature data from the USGS Gage Station at Little Falls, D.C. The regression indicated that flow was a significant predictor of the presence of a bloom; all of the blooms occurred when flow was less than 5,000 $ft^3\ sec^{-1}$ (142 $m^3\ sec^{-1}$). During the 2017 field season, there were two roughly 2-week periods without a bloom when flow was below the 5000 $ft^3\ sec^{-1}$ (142 $m^3\ sec^{-1}$) threshold found to be significant in the logistic regression. It is suspected that the water temperature in the Brunswick area was too high for a bloom to occur. Previous studies have found a lower threshold of 21°C and an upper threshold of 27°C for *P. isothrix* blooms (MD DNR, 2016b).

Survey Discussion

Survey Protocol

The survey protocol developed for this study seems to be sound; however, it is difficult to assess because the protocol was only followed in its entirety on one of the survey days. Most of the issues encountered were logistical, such as the coordination of several volunteers traveling from different areas or conflicts in the availability of volunteers who were providing drones or cameras. This was compounded by the nature

of the survey which allowed for only a few days warning once a bloom had been identified before the survey was to be completed. There were also some technical issues such as drone mechanical failures or software incompatibilities between drones, drone controllers, and computers. These issues had two impacts on the proposed surveys: a delay in start time and depletion of the limited number of available drone batteries.

The protocol called for drone flights at approximately two hours before solar noon so that the sun was high enough to illuminate the substrate but not so high as to reflect back into the drone-mounted camera. Any delay in start time increased the glare effects in the captured imagery; some datasets were lost entirely due to glare. Limited battery availability to fly the drones affected the amount of area that could be covered during a survey. False starts were common due to the complexity of calibrating a drone and a camera and starting them on the correct pre-planned flight; one flight was cancelled due to incorrectly calibrated gyroscopes, and another because the camera had not been turned on.

All of the major impediments faced during these surveys were a result of human error. If the original protocol was followed, the resulting dataset should be of much higher quality than attained by these surveys. Additionally, many of the errors were made due to a lack of familiarity with the equipment, a situation easily remedied by experience.

Data Processing Discussion

Signature Development

The spectral signatures produced by the data from the GoPro and Phantom cameras showed little variation. This can be seen in Figures 8 and 9: there is a large

amount of overlap between each band in each target spectra. The bit-depth of the processed images was 8-bit, which yields a 0 to 255 value for each band in each pixel. The signatures produced from the 16-bit images were more distinct because the value for each pixel runs from 0 to 65,535, allowing the uncompressed image to record more nuanced variations in each band.

Only three of the five available MicaSense bands were used in the signature development process because two of the bands were not effective in this environment. The Blue band was almost entirely surface reflection from water in the Potomac and few of the sub-surface features were visible through the noise. The Near IR band was mostly dark; the water absorbed the longer IR wavelengths so that there was nothing in this range reflected back to the sensor on the drone. If five bands had been available for the signature development progress, it is likely that the signatures developed for each target spectra would have been much more distinct, possibly allowing differentiation between genera of cyanobacteria and SAV.

While the failure of two of the bands to provide usable data was inconvenient for the immediate study, it did provide effective bounds on sensor range for future research. The MicaSense camera used for this project was equipped with the default filters on its sensors, but it can be ordered with other desired filters. The research from this project suggests that 525 and 725 nm are the effective lower and upper usable band ranges for recording sub-surface targets in the Potomac River. Any future research in shallow non-turbid freshwater systems would benefit from custom filters chosen from within this range, thus ensuring five usable bands.

The supervised and unsupervised classification techniques used in this project would have both benefited from additional bands. The extra bands would have aided in the differentiation of the SAV and *P. isothrix*, not accomplished in this study. Figure 20 shows the spectral signatures of *P. isothrix*, *M. wollei*, and SAV and is overlaid with four of the bands captured by the MicaSense camera. The graph shows reflectance values for every 3 nm between 340 and 820 nm, as recorded by the Satlantic Hypergun. The Near IR band records light at 840 nm, just out of the range of the Hypergun, and was not included in the graph. A 5-band camera with its default blue and Near IR filters exchanged for bands centered on 525 and 650 nm is recommended for identifying and differentiating the spectral targets in this project. This modification would ensure that all five bands were usable for targeting sub-surface features in the river and that the available bands are centered on the areas of greatest difference between the targets (Figure 21).

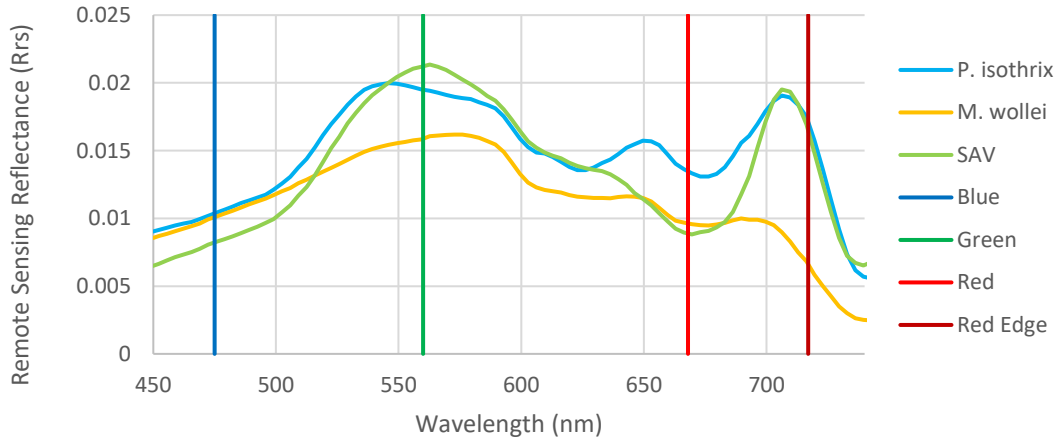

Figure 20: Spectral signatures of *P. isothrix*, *M. wollei*, and SAV overlain with the four default MicaSense bands that fall within the range of the Satlantic Hypergun. The vertical lines mark the bands captured by the current camera. The bands that line up with the largest differences between signatures are the bands most suited for differentiating the targets.

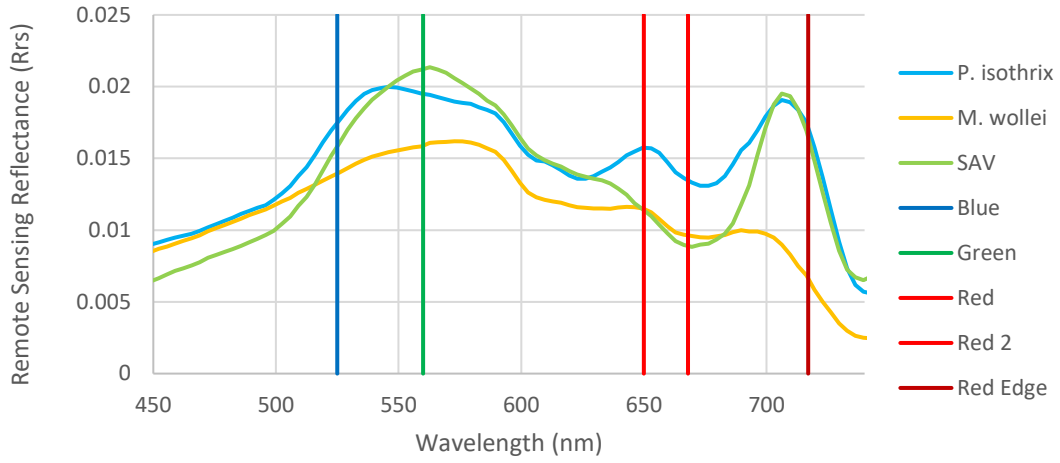

Figure 21: Spectral signatures of *P. isothrix*, *M. wollei*, and SAV overlain with the five suggested MicaSense bands. The vertical lines mark the proposed bands to be captured by a MicaSense camera. The bands were chosen to line up with the largest differences between signatures are the bands most suited for differentiating the targets.

Supervised Classification

The Parallel Piped supervised classification of the Phantom and GoPro images using the identified signatures for the target spectra was unsuccessful. The large amount of variation in the spectral signature of each target resulted in large areas of overlap, impeding the ability of the program to differentiate targets. However, the supervised classification of the MicaSense 10 m altitude imagery was able to create a good approximation of the areas of substrate and SAV, but it was unable to distinguish the SAV from the patches of *P. isothrix*. It seems that this cyanobacterium is indistinguishable from areas of shaded SAV in the three available bands.

Unsupervised Classification

The isocluster analysis unsupervised classification of 16-bit MicaSense and 16-bit Phantom images was able to differentiate substrate and SAV, but it was not able to separate SAV from *P. isothrix*. The process was disrupted in some images by areas of glare that altered the reflectance values of the targets; this was mitigated by cropping glare out of the original images. The reclassified results of the isocluster analysis, while fairly accurate, were somewhat obscured by noise from mis-identified pixels. This was probably a result of the complex colors and textures of the substrate, as well as some shadow effects.

Image Transformations

Image transformations were attempted because the supervised and unsupervised methods were very time-consuming and produced mediocre results. NGRDI and NDREI were quicker methods that resulted in a binary classification, changing each pixel to either a SAV or substrate class. It was hoped that this method would create a more accurate representation of total SAV coverage by reducing shadow and glare effects. This method requires some subjective user input on where to make a distinction between SAV and substrate; this was done with the aid of the original true color imagery.

Accuracy Assessment

The accuracy of the above methods was tested by overlaying a random sample of points with known class on the reclassified images. None of the attempted methods produced satisfactorily accurate reclassifications of the original image. All of the methods substantially overestimated SAV coverage, creating the vast majority of the errors in each

assessment. Of the attempted methods, the supervised classification was the least accurate, correctly identifying the targets 48% of the time, and the NDREI transformation was the most accurate, correctly identifying the targets 64% of the time (Table 5). The NGRDI was much more successful when applied to 16-bit Phantom images while testing the effect of altitude on accuracy, achieving 86% accuracy (Table 6). The Phantom images used in that test were captured on the only day that the protocol was successfully followed; it is likely that the minimal glare and shadow effects contributed to the better quality of the reclassification.

Modifications to Original Study Design for Accuracy Assessment

The original study called for comparing the coverage estimates of the in-water camera images to the coverage estimate of the same spatial extent cut from the 10 and 50 m altitude imagery. However, it quickly became apparent that the 10 m flight images were of sufficient quality that the target features were easily identifiable. The in-water camera images remained useful as controls to confirm identified features. This increased the amount of area that could be used to test the accuracy of the images from the area immediately surrounding each control point, where the in-water images were captured, to the entirety of the 10 and 50 m datasets. The 10 m images were very clear, and the 50 m images were fairly clear and, when in doubt, could be checked against the 10 m images. In future studies, it may be advisable to capture a much larger area at 50 m altitude and descend to 10 m only to capture images of each of the control markers.

Orthomosaics

The orthomosaics created with the images collected with the MicaSense camera during this project were not suitable for quantifying vegetation coverage. The change in reflectance values caused by sun glare was so great that normalizing the difference with an image transformation only partially corrected the problem. In addition, exposed rock reflected as strongly as the areas of densest vegetation, confounding attempts to differentiate SAV and substrate. The transformations attempted on the Phantom orthomosaics were more successful, partially because there was less glare distortion than in the MicaSense orthomosaic.

Two alterations would likely improve the orthomosaics and the information that can be obtained from them. If the protocol were followed correctly, and the aerial survey was completed two hours before solar noon, the glare effects would be greatly reduced, improving the image quality. Second, several different programs were used to process the image sets to create orthomosaics. Of the utilized programs, Drone2Map was found to produce the best quality orthomosaics. Pix4D was used to process the MicaSense images because it is the only program capable of correcting for the distortion caused by multiple lenses and recombining all of the bands into a single image. DroneDeploy (registered trademark of IBM corp., 2017) and Pix4d were also used for the Phantom images but the resulting orthomosaics were of much lower resolution. Drone2Map uses Pix4D orthorectification software, but it allows the user to export the orthomosaic in its original resolution. ArcGIS Pro was not used due to budget constraints, but it would be the ideal program for this or similar projects. ArcGIS Pro allows the user to adjust every variable in the orthorectification process. This would allow a researcher to use the non-glare

portions of images wherever there is overlap instead of averaging the pixel values, reducing much of the light effects that confounded attempts to analyze the orthomosaics.

The orthomosaics provide other benefits, despite their shortcomings. While target features were difficult to identify with software, they were easily identifiable by sight. This could allow a researcher to visually estimate vegetation coverage or the severity of a cyanobacteria bloom and would cover much more area than a visual estimate. The orthomosaic could also be revisited and analyzed by other researchers.

Relationship between Altitude and Image Resolution

Drone flight altitude requires a compromise between image resolution and area coverage. Drone flights were conducted at altitudes of 10 and 50 m; a 10 m flight requires approximately eight times as many images to cover the same amount of area as a 50 m flight. The maximum flight time for the two drones used in this project was approximately 20 minutes, meaning that area coverage potential is much higher in a 50 m flight than a 10 m flight. Initial tests with altitude and image resolution indicated that a camera altitude of 50 m would have insufficient image resolution for differentiating SAV from cyanobacteria. However, the cameras used lacked the spectral resolution to differentiate these two targets. When the focus of the research was simplified to differentiating SAV and *P. isothrix* from substrate, the range of altitudes attempted did not seem to have an effect on the accuracy of the survey. The summarized error assessment results in Table 6 indicate that the accuracy of the NGRDI transformation remained fairly constant despite changes in altitude.

Comparison with Similar Studies

Two previous studies were considered when planning the survey protocol for this research. In 2014, Flynn and Chapra published a paper describing their work using an aerial drone with a mounted RGB camera to detect *Cladophora glomerata*, a green nuisance alga. The goal of their project was very similar to this one, to differentiate major features in the survey area to reliably determine total algal coverage. The scope of their project was larger, covering 1 km of non-turbid river, and they flew at an altitude of 120 m to complete the survey in a single pass. They were able to mosaic the resulting images and differentiate target features with approximately 90% accuracy using a supervised classification method. However, *C. glomerata* seems to have been the only vegetation in the project area as the only features mentioned in their study were algae and substrate. The high altitude of the flights and resulting coarser images may have also contributed to the high accuracy of their results.

This project on the Potomac River attempted to build on their work, using similar equipment to differentiate a more diverse set of targets at much higher spatial resolution. The final results of both projects offer similar conclusions, mainly that consistent and accurate total vegetation coverage estimates are possible in shallow non-turbid waters and can be useful for studying and monitoring growth and distribution of SAV. This also probably indicates that the separation of substrate and SAV is the limit of the spectral analysis of any images captured by an RGB camera.

A project by Zwieg et al. (2014) attempted to use aerial drones to identify vegetation types in a wetland, flying a drone with an RGB camera at an altitude of 150 m and creating an orthomosaic of the resulting images. This team suffered a similar problem with glare, but it was not as detrimental to their results, because only part of their survey area was under water. They also used a supervised classification method to differentiate the vegetation communities in their study area and achieved similar results as in the supervised classification attempts in the Potomac project, i.e. very low accuracy.

Zwieg et al. solved the accuracy issue by reducing the resolution of their orthomosaic from 5 cm pixel^{-1} to 50 cm pixel^{-1}. This increased the accuracy of their classification by eliminating most of the detail that confused the classification, such as shadows and textures. This solution was appropriate to their project as the goal was to identify vegetation communities, but it was not applicable to this Potomac River project, as it would have eliminated any chance of differentiating benthic cyanobacteria from surrounding features.

Conclusion

Aerial drone imaging with a three band RGB camera is an inexpensive and practical way of assessing vegetation coverage in shallow, non-turbid, freshwater environments. With proper attention to protocol and weather, large areas can quickly be captured at sufficient resolution to observe SAV coverage and distribution and to visually search for cyanobacteria bloom presence or abundance. Given sufficient funds, a five band camera with filters to capture bands centered on 525, 560, 650, 680, and 717 nm

(Figure 21) will likely be able to differentiate substrate, SAV, and cyanobacteria coverage.

This research has demonstrated the efficacy of two methods of using UAVs to examine shallow, non-turbid, freshwater areas. Both use the same protocol and the differences in the methods are dependent on the research objectives and the available funding. The first method involves using a Phantom 3 drone with a mounted Phantom 3 camera to estimate the vegetation coverage of an area. This equipment can be used to capture 24-bit DNG images of an area from an altitude of 50m. An orthomosaic can be created from these images using Drone2Map software. The orthomosaic can then be transformed using Terrset or a similar program and the NGRDI formula to differentiate areas of vegetation from areas of substrate. The resulting image can then be reclassified into a binary image divided into vegetation and substrate, and it can provide total vegetation coverage estimates for the project area. The drone with a mounted camera should cost approximately $800, Terrset software $1,250 (but academic and student licenses are cheaper), and Drone2Map $3,500 for a one-year subscription.

The second method involves using a 3DR SOLO with a mounted MicaSense RedEdge camera to differentiate and quantify coverage of spectral targets in an area. The filters on the MicaSense RedEdge can be customized as desired; the proposed bands in Figure 21 are specific to the spectral targets of interest in the Brunswick, MD area of the Potomac River. The spatial resolution of the MicaSense camera is lower than that of the Phantom camera, but an altitude of 50 m may still be low enough to differentiate targets depending on the goals of the study; if higher resolution is needed, an altitude of 10 m may be more appropriate. An orthomosaic can be created from these images using

Drone2Map software. Terrset should then be used to perform an isocluster analysis of all data from the five available bands. The resulting image will be automatically classified into spectrally similar groups; these groups can be compared with a true color image of the project area to determine which of the spectral targets they most correspond to as was done in Figure 11. An isocluster analysis was found to be the best option for differentiating targets in this study, but a supervised classification may be better suited to differentiating multiple targets. Terrset could be used to perform a supervised classification utilizing all five of the available bands and using features in the control points as training areas. The 3DR SOLO drone costs approximately $300 and a MicaSense RedEdge camera $4,900; costs of Terrset and Drone2Map are the same as above.

Proposed Future Work

Benthic Autotroph Coverage

This study made progress towards the original goal of quantifying benthic autotroph coverage in the Upper Potomac, but it was unable to obtain an estimate for submerged plant growth. Here I describe the methodology I believe will be the most successful in quantifying benthic autotroph coverage in the future.

Using the methods described in the conclusion, an attempt should be made to estimate benthic autotroph coverage in a portion of the River. Four 20-minute flights at an altitude of 10 m should be able to cover a 50 x 200 m transect across the Potomac, a single fifth 50 m altitude flight should be able to cover the same spatial area. These five flights should be completed with both a MicaSense RedEdge camera and a Phantom 3

camera. Four orthomosaics should be completed from the collected images; one at each altitude for each camera.

ArcGIS Pro (ESRI, 2018) is developing tools that allow better control over how orthomosaics are constructed. This program may be able to eliminate some of the image glare problems by allowing the researcher to choose which pixels are represented in areas of overlap between images instead of averaging the values. If a researcher were able to choose to keep the lowest reflectance values in overlap areas and discard higher values, there should be no glare effects.

A supervised classification, using known benthic autotroph locations from control points, should then be used to identify spectral targets in the project area. Classification accuracy can be assessed using sample points and an error matrix as was done above. If low accuracy is attained, additional training areas should be identified using the low altitude imagery and the control point images. When high classification accuracy is achieved, above 80%, total coverage of each target in the survey area can be quantified.

Further work should to be done to determine how much of the Potomac can be characterized based on a survey such as the one described, which covers approximately 10,000 m^2. This could be accomplished with several simultaneous drone surveys along a stretch of river or by comparing the results of the drone surveys with the results of nearby traditional visual surveys.

Spectral Library

A library should be collected containing the spectral signatures of common autotrophs and substrate types in the Upper Potomac. These spectral signatures should be

collected with a radiometer such as the Satlantic Hypergun. This library would allow future researchers to better decide which camera or camera filters would be best for differentiating targets, as was done with the MicaSense RedEdge camera for the known spectral targets in the Brunswick area. Bands should be chosen to collect reflectance in the areas of the spectrum that show the largest differences in the spectral signatures of the targets.

Hyperspectral Camera

Drone-mounted hyperspectral cameras are expensive but if one were available it would provide imagery that would almost certainly be able to differentiate all spectral targets in the Upper Potomac. A hyperspectral camera records images with hundreds of bands for each pixel, i.e. one band for every 3 nm, providing much better spectral resolution. The spectral resolution may even be sufficient to differentiate between species of SAV or cyanobacteria, between new growth and old growth of the same species, and to estimate thickness of benthic cyanobacteria or macroalgal mats. Data collected with a hyperspectral camera could also be used to identify spectral signatures which could be incorporated into a spectral library such as described above. Terrset IDRISI is capable of processing hyperspectral data and can perform both unsupervised and supervised classifications.

Benthic Cyanobacteria Toxicity

If benthic autotroph coverage can be quantified and SAV can be differentiated from benthic cyanobacteria, it may be possible to estimate cyanotoxin levels in the water.

This would require multiple drone surveys a day throughout a cyanobacteria bloom and simultaneous collection and toxin analysis of water and cyanobacteria samples. With these data, it may be possible to establish a correlation between cyanobacteria coverage and levels of dissolved toxin. Cyanotoxins are mainly released during senescence (Carpenter et al., 1986), so it may be necessary to estimate coverage of both healthy and senescing cyanobacteria. If it is possible to estimate biomass of spectral targets with hyperspectral data, a better correlation could be expected.

APPENDIX I

Data Processing Protocol

1. RAW to 16-bit TIFF compatible with ArcMap and Terrset
    a. Adobe Lightroom
        i. File
            1. Import Photos and Video
                a. Select RAW Files
                    i. Export as TIFF
                    ii. No compression
                    iii. AdobeRGB (1998) Color Space
                    iv. 16 bits/component
2. Crop to same spatial extent
    a. ArcMap
        i. Add 8 and 16 bit images
        ii. Draw toolbar
            1. Draw rectangle around spatial extent of lowest altitude image
                a. Select ‘Convert Graphics to Features’ on Draw toolbar
                    i. Save as shape file
        iii. Change transparency of lowest altitude image to 50% and place first in the drawing order
        iv. Place image from higher altitude second in drawing order
        v. Open Georeferencing toolbar
            1. Use ‘Shift’ and ‘Scale’ tools to align reference markers in the images
                a. Update Georeferencing when aligned
        vi. Windows
            1. Image Analysis
                a. Select image and rectangular shapefile
                    i. Export (if 16-bit TIFF original)
                        1. Selected Graphics (Clipping)
                        2. Compression type: None
                        3. Format: TIFF
                    ii. Export (if JPEG original)
                        1. Selected Graphics (Clipping)
                        2. Compression Type: JPEG
                        3. Compression Quality: 100

3. NGRDI (Normalized Green Red Difference Index)
    a. Terrset
        i. IDRISI GIS Analysis
            1. Mathematical Operators
                a. OVERLAY
                    i. First-Second/First+Second
                        1. First band is Green band
                        2. Second band is Red band
                        3. Output image is NGRDI
            2. Database Query
                a. RECLASS
                    i. Use aerial and transformed image to find point in -1 to 1 scale where substrate gives way to vegetation
                    ii. Reclass values below this point as substrate, reclass values above this point as vegetation
                        1. Assign a common palette to each image to ease interpretation
4. NDREI (Normalized Difference RedEdge Index)
    a. Terrset
        i. IDRISI GIS Analysis
            1. Mathematical Operators
                a. OVERLAY
                    i. First-Second/First + Second
                        1. First band is RedEdge band
                        2. Second band is Red band
                        3. Output image is NDREI
            2. Database Query
                a. RECLASS
                    i. Use aerial and transformed image to find point in -1 to 1 scale where substrate gives way to vegetation
                    ii. Reclass values below this point as substrate, reclass values above this point as vegetation

5. ISOCLUSTER (Unsupervised Classification)
    a. Terrset
        i. IDRISI Image Processing
            1. Hard Classifiers
                a. ISOCLUST
                    i. Enter all available bands
                    ii. Enter ‘20’ as number of desired categories
                    iii. Output image is isocluster analysis
        ii. File
            1. Display
                a. Symbol workshop
                    i. Open Palette
                        1. Beginning in square 0 at top left and moving right choose, color scheme for isocluster reclassification
                        2. Example: Square 1 is Dark Green and will correspond to isocluster classes identified as SAV
        iii. File
            1. Data Entry
                a. Edit
                    i. Enter a single column numbered 1 through 20
                    ii. Save as Attribute Values File (AVL File)
                    iii. Create Raster Group with True color image and isocluster output
                    iv. Link images
                    v. Enter one space after each number in first column and enter category number from palette file based on visual identification of isocluster classes by comparison with linked true color image
                b. Assign
                    i. Feature definition image is Isocluster
                    ii. Feature output is reclassed image
                    iii. Attribute Values File is from above step after all 20 classes have been reclassified with numbers corresponding to custom palette

iv. Layer Properties
    1. Palette File
        a. Choose palette file created above
        b. Resulting image is reclassed isocluster image with palette colors reflecting desired categories

6. Error Assessment
    a. Terrset
        i. IDRISI Image Processing
            1. Accuracy Assessment
                a. SAMPLE
                    i. Reference image is true color image
                    ii. Select Stratified random sampling scheme
                    iii. Number of points: 50
                    iv. Output file as desired
                    v. Vector output type
        ii. File
            1. Data Entry
                a. Edit
                    i. Open new AVI file
                    ii. Number through 50 followed by a space
            2. Display
                a. Choose true color image
                    i. Add layer
                        1. Add sample vector file
                            a. Identify class of each of 50 vector locations based on true color image and enter in AVI file
            3. File
                a. Reformat
                    i. RASTERVECTOR
                        1. Select sample vector set
                        2. Let file to be updated blank
                            a. Create new image file
                            b. Copy spatial extent from true color image
                b. Data Entry
                    i. Assign
                        1. Feature definition image is rasterized sample location file
                        2. Feature output is reclassed sample file

3. Attribute Values File is from above step after all 50 sample locations have been assigned a class based on the true color image

iii. IDRISI Image Processing
    1. Accuracy Assessment
        a. ERRMAT
            i. Ground truth image is reclassed sample raster
            ii. Categorical map image is either a reclassed isocluster of the true color image or a transformed version of the true color image
            iii. Output consists of a confusion matrix detailing correctly and incorrectly classed sample locations as well as an overall accuracy estimate

APPENDIX II

Bloom Occurrence Statistics

A binary logistic regression was performed to examine the relationship between Potomac River flow, water temperature, and cyanobacteria blooms in the portion of the Potomac near Brunswick, MD. River flow data were obtained from the Point of Rocks USGS Gage station located near Point of Rocks, MD, approximately 10 km downstream from Brunswick. Water temperature data were obtained from the Little Falls USGS Gage station near Washington D.C., approximately 75 km downstream from Brunswick. A linear regression was performed to examine the relationship between the water temperature at Little Falls and Brunswick to determine whether the Little Falls temperature data were a valid proxy for the temperatures at Brunswick.

Water Temperature Linear Regression

Brunswick water temperature data were collected on each of the five survey days in the summer of 2017. Thirty-six additional data points were obtained from MD DNR survey data collected by J. Henesy of MD DNR during a Potomac River monitoring project conducted between 2013 and 2016. A linear regression was performed to determine if the water temperature in the two areas was significantly correlated, by comparing water temperature measurements taken at Brunswick to the water temperature recorded at Little Falls on that day. The water temperature data are located in Table AII-1.

The data met all of the assumptions necessary to validate a linear regression; the Little Falls data were used as the independent variable and the Brunswick data were the dependent variable. The variables have a linear relationship as can be seen in Figure AII-

1, both variables were distributed normally, and the data exhibit a homoscedastic distribution. The results of the SPSS regression calculations can be found in Tables AII-2, 3, and 4. The null hypothesis was that there is no relationship between the water temperature at Little Falls and the water temperature at Brunswick.

Table AII-1: Water temperature data measured manually at Brunswick and automatically at the Little Falls USGS Gage Station.

Date	Brunswick	Little Falls	Date	Brunswick	Little Falls	Date	Brunswick	Little Falls
5/30/13	23.4	21.8	6/26/14	24.0	26.3	6/2/16	25.6	26.9
6/5/13	23.3	23.7	7/3/14	25.1	28.4	6/15/16	23.8	26
6/11/13	23.8	22	7/21/14	25.6	25.9	6/29/16	26.2	27.9
6/19/13	23.5	23.5	7/29/14	23.3	25.8	7/13/16	27.8	30.1
6/27/13	26.6	27.8	8/14/14	24.4	23.9	7/27/16	29.6	32.6
7/10/13	27.6	28.4	8/21/14	23.9	25.9	8/10/16	26.4	29.1
7/23/13	29.5	29.6	9/18/14	19.6	21.8	8/24/16	26.9	28.6
7/30/13	26.0	25.7	5/7/15	17.5	22.3	9/7/16	26.1	27.5
8/7/13	23.6	24.9	6/1/15	21.5	29.5	6/12/17	24.3	28.3
8/14/13	23.5	26.3	6/17/15	22.2	29.4	6/30/17	27.4	28.8
8/26/13	25.1	25.1	7/1/15	25.5	23.2	8/18/17	25.5	29.4
9/18/13	21.0	21.1	7/29/15	27.6	31.1	8/25/17	24.7	28.7
6/4/14	21.0	23.2	8/17/15	29.0	30.4	9/28/17	23.9	27.1
6/11/14	23.8	22.4	9/9/15	29.4	29.6			

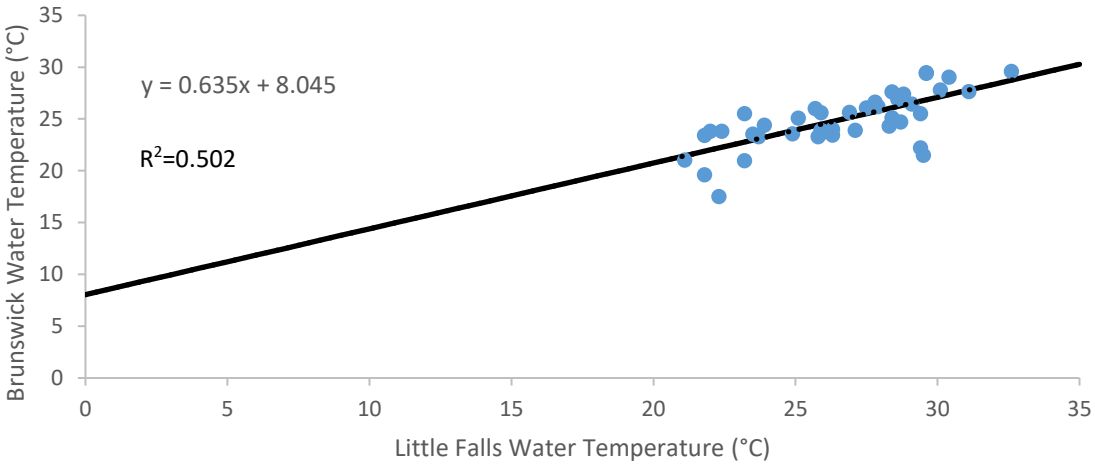

Figure AII-1: Water temperature data from each station plotted against each other and overlain with the regression line generated by SPSS. The Little Falls water temperature was the independent variable and the Brunswick water temperature measurements were the dependent variable.

Table AII-2 contains the SPSS generated model summary of the linear regression of the water temperature data from Brunswick and Little Falls. The R, R^2, and adjusted R^2 values indicate the correlation between the independent and dependent variables; R^2 is the square of the R score and the Adjusted R^2 score penalizes the R^2 score based on the number of independent variables included in the model. An Adjusted R^2 of 0.479 indicates that 47.9% of the variability of the dependent variable is accounted for by the independent variable. The standard error of the residual is the square root of the residual mean square located in Table AII-3.

Table AII-2: SPSS generated model summary of the linear regression.

R	R^2	Adjusted R^2	Std. Error of the Estimate
0.708	0.502	0.489	1.882

Table AII-3 contains the SPSS generated Analysis of Variance of the linear regression. The Sum of Squares column details the square of the difference between each datum and the regression line. The Regression Sum of Squares is the variance that can be explained by the independent variable while the Residual Sum of Squares is the variance that cannot be explained by the independent variable. The Total Degrees of Freedom are equal to N - 1 where N is the number of data in the sample. The Regression Degrees of Freedom are equal to the number of coefficients in the model – 1; in this model, there are two coefficients (the Y-intercept and the slope). The Residual Degrees of Freedom are equal to the Total Degrees of Freedom – the Regression Degrees of Freedom. The F-score was obtained by dividing the Regression Mean Square by the Residual Mean Square and has an associated p-value based on the degrees of freedom and the desired alpha error of 0.05%. The F-score of 39.27 surpasses the F-table threshold of 4.08 and indicates that the null hypothesis can be rejected, with a 0.1% chance of an alpha error.

Table AII-3: SPSS generated Analysis of Variance of the linear regression.

	Sum of Squares	Degrees of Freedom	Mean Square	F-score	Significance
Regression	139.03	1	139.03	39.27	.001
Residual	138.073	39	3.54		
Total	277.103	40			

Based on the F-score and the R^2-score, this linear regression suggests that the water temperature at Brunswick is highly correlated with the water temperature at Little Falls. The regression describing the relationship between the water temperature in the two areas is explained in Table AII-4. The line for the regression is built from the coefficient column, Brunswick Temperature = 8.045 + 0.632Little Falls Temperature;

this is the regression line graphed in Figure AII-1. The standard error and confidence interval columns show the variability within the relationship. A t-score is given for both the Y-intercept and the slope. These t-scores describe whether the respective coefficients are significantly different from 0; a coefficient of 0 would indicate that there was no correlation between the independent and dependent variables. The t-score of 0.005 for the Y-intercept indicates that there is a significant relationship with a 0.5% chance of an alpha error. The t-score of 0 for the slope indicates that the relationship between the independent and dependent variables is significant with a 0% chance of an alpha error.

Table AII-4: SPSS generated linear regression model coefficients.

	Unstandardized Coefficients		Standardized Coefficients	t-score	Sig.	95.0% Confidence Interval for Coefficient	
	Coefficient	Std. Error	Coefficient			Lower Bound	Upper Bound
Y-intercept	8.045	2.696		2.984	0.005	2.591	13.498
Slope	0.632	0.101	0.708	6.267	0	0.428	0.836

Potomac River Flow and Water Temperature Binary Regression

A binary logistic regression was performed to determine the relationship between Potomac River Flow, water temperature, and the presence of a benthic cyanobacteria bloom. This statistical test was chosen because the aerial drone surveys failed to provide quantitative coverage estimates of benthic cyanobacteria in the Potomac. The available data for the survey period (May – October, 2017) consisted of daily average flow data from the USGS Point of Rocks Gage Station, daily average water temperature data from the USGS Little Falls Gage Station, and cyanobacterial bloom presence/absence data. The binary logistic regression is the only statistical test capable of analyzing two

independent variables consisting of ratio data and a dependent variable consisting of binary categorical data.

The data met all of the assumptions necessary to validate a binary logistic regression; the independent variables consisted of scale data and the dependent variable consisted of two mutually exclusive categories. The Little Falls water temperature data and the Point of Rocks flow data were used as the independent variables and the Brunswick bloom presence-absence data were used as the dependent variable. The results of the SPSS regression calculations can be found in Tables AII-5-10. The null hypothesis was that there is no relationship between flow and water temperature and cyanobacteria blooms during the period May – October, 2017 at Brunswick, MD.

The SPSS binary regression program begins by defaulting to an assumption that will result in the best prediction of the known data (Table AII-5). The program assumed that there would not be any cyanobacteria blooms that allowed the program to correctly guess 81.5% of the cases. Tables AII-6 and 7 contain additional output for the null model. Table AII-6 contains the coefficient and standard error for the null model; the Wald statistic is obtained by dividing the coefficient by the standard error. The resulting Wald statistic is compared to a chi square critical values table for 1 degree of freedom and a p-value of 0.05 to get a significance value. The significance value of $p < 0.001$ generated by SPSS implies that the null hypothesis can be rejected with a 0.1% chance of alpha error.

Table AII-5: SPSS generated classification table output.

Observed		Predicted		Percentage Correct
		No Bloom	Bloom	
	No Bloom	123	0	100.0
	Bloom	28	0	.0
	Overall Percentage			81.5

Table AII-6: SPSS generated null model significance output.

Coefficient	Std. Error	Wald	Degrees of Freedom	Significance
-1.480	0.209	49.957	1	0.001

The preliminary results in Tables AII-5 and 6 reject the null hypothesis that there is no relationship between the independent and dependent variables. The SPSS output in Tables AII-7, 8, 9, and 10 explain the relationship between the independent and dependent variables. Table AII-7 contains the likelihood that the addition of the independent variables will improve the model. The flow and water temperatures both significantly improve the model; flow with a 0.0% chance of alpha error and water temperature with a 0.5% chance of alpha error; the addition of both variables entails a 0.2% chance of alpha error. The Hosmer-Lemeshow goodness-of-fit statistic rates how well the model fits the data; the chi-square score of 5.857 was not significant (Table AII-8). The non-significant chi-square value of this test indicated that the data fit the model. This test was accomplished by sub-sampling the dataset to see if the proportions of bloom to no bloom data remained the same as in the overall model.

Table AII-7: SPSS generated output detailing the whether the addition of independent variables significantly improves the model.

		Score	Degrees of Freedom	Significance
	Flow	12.489	1	0.001
Variables	Water Temp	7.817	1	0.005
Overall Statistics		12.718	2	0.002

Table AII-8: SPSS generated Hosmer-Lemeshow goodness-of-fit statistic.

Chi-square	Degrees of Freedom	Sig.
5.857	8	0.663

Table AII-9 illustrates the efficacy of the SPSS generated model and Table AII-10 shows the significance of the independent variables as well as the coefficients for the model formula. Table AII-9 is very similar to Table AII-5, but this table uses the SPSS generated model instead of placing all cases in whichever category resulted in a higher accuracy prediction. The model correctly predicted 86.1% of the cases while the null model correctly predicted 81.5% of the cases. Table AII-10 contains the coefficients for each independent variable and the Y-intercept, which were inserted into a logistic regression formula to create the binary regression model: Probability of Bloom = $(1 + \exp(-(-0.002 * \text{Flow} + 0.241 * \text{Water Temperature} - 2.767)))^{-1}$. The significance values attached to the independent variables reject the null hypothesis that there is no relationship between the independent and dependent variables.

Table AII-9: SPSS generated classification table output with independent variables included.

Observed		Predicted		Percentage Correct
		No Bloom	Bloom	
	No Bloom	117	6	95.1
	Bloom	15	13	46.4
Overall Percentage				86.1

Table AII-10: SPSS generated binary regression formula.

Variable	Coefficient	Std. Error	Wald	Degrees of Freedom	Significance
Flow	-0.002	0.000	14.949	1	0.001
Water Temp	0.241	0.108	5.007	1	0.025
Y-intercept	-2.767	2.509	1.216	1	0.270

WORKS CITED

Literature

Alexander, D. J., Hart, D. E., & Marsden, I. D. (2008). Evaluation and development of techniques to map macroalgae in the Avon-Heathcote Estuary Ihutai. *Estuarine Research Report, 35*.

Anker, Y., Hershkovitz, Y., Ben Dor, E., & Gasith, A. (2014). Application of aerial digital photography for macrophyte cover and composition survey in small rural streams. *River Research and Applications, 30*(7), 925-937.

Beaulieu, M., Pick, F., & Gregory-Eaves, I. (2013). Nutrients and water temperature are significant predictors of cyanobacterial biomass in a 1147 lakes dataset. *Limnology and Oceanography*, *58*(5), 1736-1746.

Blazer, V., Iwanowicz, L., Henderson, H., Mazik, P., Jenkins, J., Alvarez, D., & Young, J. (2012). Reproductive endocrine disruption in smallmouth bass (*Micropterus dolomieu*) in the Potomac River basin: Spatial and temporal comparisons of biological effects. *Environmental Monitoring & Assessment*, *184*(7), 4309-4334. doi:10.1007/s10661-011-2266-5

Carpenter, S. R., & Lodge, D. M. (1986). Effects of submersed macrophytes on ecosystem processes. *Aquatic Botany, 26*, 341-370.

Davie, A. W., Mitrovic, S. M., & Lim, R. P. (2012). Succession and accrual of benthic algae on cobbles of an upland river following scouring. *Inland waters, 2*(2), 89-100.

Dean, C. A., & Selckmann, G. M. (2015). Ecology and Management of Filamentous Green Algae. *ICPRB Report, 15*-7, Rockville, MD, pp. 4-7.

Ferrão-Filho, A. S., & Kozlowsky-Suzuki, B. (2011). Cyanotoxins: Bioaccumulation and effects on aquatic animals. *Marine Drugs*, 9(12), 2729-2772. doi:10.3390/md9122729

Flynn, K. F., & Chapra, S. C. (2014). Remote sensing of submerged aquatic vegetation in a shallow non-turbid river using an unmanned aerial vehicle. *Remote Sensing*, *6*(12), 12815-12836.

Funari, E., & Testai, E. (2008). Human health risk assessment related to cyanotoxins exposure. *Critical Reviews in Toxicology*, *38*(2), 97-125. doi:10.1080/10408440701749454

Gholizadeh, M. H., Melesse, A. M., & Reddi, L. (2016). A comprehensive review on water quality parameters estimation using remote sensing techniques. *Sensors*, *16*(8), 1298.

Hanington, P., Rose, A., & Johnstone, R. (2016). The potential of benthic iron and phosphorus fluxes to support the growth of a bloom forming toxic cyanobacterium *Lyngbya majuscula*, Moreton Bay, Australia. *Marine and Freshwater Research*, *67*(12), 1918-1927.

Hudson, C. & J. Mattheiss. (2017). Microcystin transfer in the Potomac foodweb. Presentation, US EPA Region III Harmful Algae Technical Workshop, December 6, 2017, Philadelphia, PA.

Kurmayer, R., Deng, L., & Entfellner, E. (2016). Role of toxic and bioactive secondary metabolites in colonization and bloom formation by filamentous cyanobacteria *Planktothrix*. *Harmful Algae*, *54*, 69-86.

Levin, N., Ben-Dor, E., & Singer, A. (2005). A digital camera as a tool to measure colour indices and related properties of sandy soils in semi-arid environments. *International Journal of Remote Sensing*, *26*(24), 5475-5492.

Marcus, W. A., & Fonstad, M. A. (2008). Optical remote mapping of rivers at sub-meter resolutions and watershed extents. *Earth Surface Processes and Landforms*, *33*(1), 4-24.

Maryland Department of Natural Resources [MD DNR] Eyes on the Bay (2016a). Potomac River Water Quality and Habitat Assessment Summary available on the World Wide Web (USGS Water Data for the Nation), accessed [February 14, 2017], at URL [http://eyesonthebay.dnr.maryland.gov/eyesonthebay/documents/Potomac_WQassessment_handout-Sep2016.pdf].

Maryland Department of Natural Resources [MD DNR], Fisheries and Boating Services, Freshwater Monitoring and Assessment Division - Freshwater Fisheries (2016b). Survey and management of Maryland's fishery resources: Annual performance report 2015. (U.S. Fish & Wildlife Service Federal Aid Project F-48-R-26). Maryland Department of Natural Resources, Annapolis, MD.

Miller, M. A., Kudela, R. M., Mekebri, A., Crane, D., Oates, S. C., Tinker, M. T., Staedler, M., Miller, W. A., Toy-Choutka, S., Dominik, C., Langlois, G., Murray, M., Ward, K., Jessup, D., & Hardin, D. (2010). Evidence for a novel marine harmful algal bloom: cyanotoxin (microcystin) transfer from land to sea otters. *PLoS One*, *5*(9), e12576.

Moyer, D.L., Langland, M.J., Blomquist, J.D., and Yang, G, (2017). Nitrogen, phosphorus, and suspended-sediment loads and trends measured at the Chesapeake Bay Nontidal Network stations: Water years 1985-2016, U.S. Geological Survey data release, https://doi.org/10.5066/F7RR1X68.

Nezlin, N. P., Kamer, K., & Stein, E. D. (2007). Application of color infrared aerial photography to assess macroalgal distribution in an eutrophic estuary, Upper Newport Bay, California. *Estuaries and Coasts, 30*(5), 855-868.

Niemann, T. (2017). PTLens 9.0 [Computer Software] Portland, OR: EPaperPress. Retrievable from http://epaperpress.com/ptlens/index.html.

Paerl, H., & Otten, T. (2013). Harmful cyanobacterial blooms: Causes, consequences, and controls. *Microbial Ecology*, *65*(4), 995-1010. doi:10.1007/s00248-012-0159-y

Rogers, E. D., Henry, T. B., Twiner, M. J., Gouffon, J. S., McPherson, J. T., Boyer, G. L., Sayler, S., & Wilhelm, S. W. (2011). Global gene expression profiling in larval zebrafish exposed to microcystin-LR and microcystis reveals endocrine disrupting effects of Cyanobacteria. *Environmental Science & Technology*, *45*(5), 1962-1969. doi:10.1021/es103538b

U.S. EPA (United States Environmental Protection Agency). 2015. Health Effects Support Document for the Cyanobacterial Toxin Microcystins. EPA 820R15102, Washington, DC; June, 2015. Available from:http://water.epa.gov/ drink/ standards/hascience.cfm

U.S. Geological Survey, 2017, National Water Information System data available on the World Wide Web (USGS Water Data for the Nation), accessed [March 15, 2017], at URL [http://waterdata.usgs.gov/nwis/].

Van der Merwe, D., & Price, K. P. (2015). Harmful algal bloom characterization at ultra-high spatial and temporal resolution using small unmanned aircraft systems. *Toxins*, *7*(4), 1065-1078.

Visser, F., Wallis, C., & Sinnott, A. M. (2013). Optical remote sensing of submerged aquatic vegetation: Opportunities for shallow clear-water streams. *Limnologica-Ecology and Management of Inland Waters, 43*(5), 388-398.

World Health Organization. (1998). Guidelines for drinking-water quality. Vol. 2, Health criteria and other supporting information: addendum. Geneva, Switzerland, 95-110.

Yong Q., T., Qian, Y., Zimmerman, M. J., Flint, S., & Waldron, M. C. (2010). Differentiating aquatic plant communities in a eutrophic river using hyperspectral and multispectral remote sensing. *Freshwater Biology*, *55*(8), 1658-1673. doi:10.1111/j.1365-2427.2010.02400.x

Zweig, C. L., Burgess, M. A., Percival, H. F., & Kitchens, W. M. (2015). Use of unmanned aircraft systems to delineate fine-scale wetland vegetation communities. *Wetlands*, *35*(2), 303-309.2), 303-309.

Software

Adobe Systems Inc. (2017). Adobe Lightroom for Windows, version 2.0. San Jose, California: Adobe Systems Inc.

ArduPilot. (2017). Mission Planner for Windows, version 1.3.50. Retrieved from http://ardupilot.org/planner/index.html.

Clark Labs. (2017). TerrSet for Windows, version 18.3. Worchester, MA: Clark Labs.

ESRI. (2017). ArcGIS for Windows, version 10.4. Redlands, CA: Environmental Systems Research Institute.

ESRI. (2017). Drone2Map for Windows, version 1.3. Redlands, CA: Environmental Systems Research Institute.

IBM Corp. (2013). IBM SPSS Statistics for Windows, version 23.0. Armonk, NY: IBM Corp.

Infatics, Inc. (2017). DroneDeploy for Windows, version 2.0. San Francisco, CA: DroneDeploy.

Pix4D. (2017). Pix4Dmapper for Windows, version 3.3.19. Lausanne, Switzerland: Pix4D.

Hardware

3DR. (2017). 3DR SOLO Unmanned Aerial Vehicle. Berkeley, California: 3D Robotics Inc.

DJI. (2017). Phantom 3 Unmanned Aerial Vehicle with mounted Phantom 3 camera. Shenzhen, Guangdong, China: Da-Jang Innovations Science and Technology Co. Ltd.

GoPro Inc. (2017). GoPro Hero 4 Black. San Mateo, California: GoPro Inc.

MicaSense Inc. (2017). RedEdge-M multispectral sensor. Seattle, Washington: MicaSense, Inc.